CO-PRODUCTION OF CHITIN NANOFIBERS, PROTEINS, AND LIPIDS IN MARINE DIATOMS BELONGING TO THE *THALASSIOSIRA* GENUS

A Thesis Submitted to
the Graduate School of
İzmir Institute of Technology
in Partial Fulfillment of the Requirements for the Degree of

MASTER OF SCIENCE

in Environmental Engineering

by
TUĞÇE SEZGİN

June 2022
İZMİR

ACKNOWLEDGEMENTS

Particularly, I would like to express my sincere appreciation to my supervisor Assist. Prof. Dr. Altan ÖZKAN for his advice, guidance, support, motivation, encouragement, patience, and trust throughout my graduate studies.

I would like to thank my thesis defense committee members Assoc. Prof. Dr. Sırma YEĞİN and Assist. Prof. Dr. Mehmet Ali KÜÇÜKER for their valuable recommendations.

I would like to express my special thanks to my best friend Emre ÇALHAN for his endless support, insightful comments, and advice during my whole life. This study would not have been completed without his support. I am deeply thankful to Dilruba DAL for her precious friendship and help in the instrumental analysis of the study.

Lastly, I would like to thank my mother Safiye SEZGİN, my sister Esra ERDOĞAN and her kind husband Ali ERDOĞAN, and my brother Ersin SEZGİN for their support, encouragement, and trust.

ABSTRACT

CO-PRODUCTION OF CHITIN NANOFIBERS, PROTEINS, AND LIPIDS IN MARINE DIATOMS BELONGING TO THE *THALASSIOSIRA* GENUS

Chitin is a biopolymer used in various industries, including biomedical, pharmaceutical, medical, and food. Today, the vast majority of chitin is obtained from waste shellfish. Shellfish chitin has an inherent impurity problem because chitin in these organisms is embedded in other organics and inorganics. Thus, new sources have been investigated. Diatoms, particularly *Thalassiosira* and *Cyclotella* species, have the potential to be the providers for applications requiring high quality through their unique ability to biosynthesize and extrude chitin nanofibers. The primary aim of this study is to study this potential. This investigation entailed the cultivation of three *Thalassiosira* strains according to a standard cultivation protocol under photobioreactor conditions. The secondary aim was to assess the possibility of commercially valuable co-product generation. For this, biomass protein, lipid, and fatty acids contents were analyzed. Chitin productivity varied significantly between the strains. The peak productivities and final concentrations ranged from 4 to 25 mg/L-day and from 60 to 250 mg/L, respectively. Average fiber diameters ranged from 68.5 to 95.0 nm. Silicon limited growth increased the chitin biosynthesis in *T.weissflogii* 1336 and *T.pseudonana* 2135. Biomass lipid contents of over 45% were obtained with *T.pseudonana* 2135 under silicon depletion. The fatty acid profiles indicated the suitability for application as live aquaculture feed for *T.weissflogii* 1336, and biodiesel feedstock material for *T.pseudonana* 2135. The highest biomass protein contents were about 30%, which were obtained under silicon availability. This study, for the first time, assessed the chitin productivity of *Thalassiosira* strains and demonstrated unique multiproduct generation scenarios.

ÖZET

THALASSIOSIRA CİNSLERİNE AİT DENİZ DİATOMLARINDA KİTİN NANOLİFLERİNİN, PROTEİNLERİN VE LİPİDLERİN EŞ ZAMANLI ÜRETİMİ

Kitin biyomedikal, eczacılık, tıp ve gıda endüstirilerinde kullanılan bir biyopolimerdir. Günümüzde kitin kabuklu deniz canlılarından elde edilmektedir. Ancak kitin bu canlılarda başka organiklere ve inorganiklere kimyasal bağlarla bağlıdır. Bu durum elde edilen kitinde safsızlık problemlerine yol açmaktadır. Doğada kitini en saf şekilde üreten ve hücre dışına nanofiber olarak çıkaran tek canlı *Cyclotella* ve *Thalassiosira* cinsine ait diatomlardır. Bu sebeple piyasadaki mevcut kitin ihtiyacını karşılayabilmek adına eşsiz bir potensiyele sahiptir. Bu çalışmanın ilk amacı *Thalassiosira* cinsine ait 3 farklı diatom suşunda kitin nanofiber özelliklerini belirleyerek yüksek kalite gerektiren uygulamalar için potansiyelini incelemektir. İkinci amaç ise ticari olarak kullanılabilecek yan ürün oluşturma özelliklerini değerlendirmektir. Bu sebeple diatomlar standart koşullarda kabarcık kolon fotobiyoreaktörde silikon varlığındaki ve silikon yokluğundaki üretkenlik kıyaslaması için iki aşamalı olarak yetiştirilmiştir. Kültivasyon süresi boyunca biyokütle, protein, lipid ve yağ asitleri analizleri yapılmıştır. Kitin üretkenlikleri suşlar arasında önemli farklılıklar gösterdiği belirlenmiştir. Maksimum üretkenlikler ve final konsantrasyonları, sırasıyla 4 ile 25 mg/L-gün ve 60 ile 250 mg/L aralığında bulunmuştur. Ortalama fiber çapları ise 68.5 ile 95.0 nm arasında değişmektedir. Silikonsuz ortam *T.weissflogii* 1336 ve *T.pseudonana* 2135 suşlarında kitin biyosentezini arttırmıştır. *T.pseudonana* 2135 suşunun ortamdaki silikon tükendikten sonra biyokütledeki lipid içeriği %45'in üzerinde elde edilmiştir. Yağ asidi profilleri, *T.weissflogii* 1336 için akuakültür yemi olarak ve *T.pseudonana* 2135 için ise biyodizel besleme stoğu materyali olarak uygulamaya uygun olduğunu göstermiştir. En yüksek biyokütle protein içerikleri, silikon mevcut ortamda yaklaşık %30 olarak elde edilmiştir. Bu çalışmada, ilk kez *Thalassiosira* suşlarının kitin üretkenliği ve yan ürün olarak lipid ve protein içerikleri değerlendirilmiştir.

TABLE OF CONTENTS

LIST OF FIGURES

Figure **Page**

LIST OF TABLES

CHAPTER 1

INTRODUCTION

Microalgae are a group of primarily single cellular photosynthetic microorganisms. Diatoms are one of the major groups which differentiate themselves from the rest with their distinct silica-based cell walls (T. Lebeau and Robert 2003b). They are usually planktonic, meaning they grow suspended in aqueous media. They need a light source to drive their metabolic activities and also a range of nutrients for metabolic reactions. Microalgae require carbon, nitrogen, and phosphorus as macronutrients. In addition to these, diatoms need a silicon source in the form of silicic acid ($Si(OH)_4$) for cell wall formation (Tréguer et al. 1995). They are acclimated to maintain high photosynthetic efficiencies under unsteady environmental conditions and at low nutrient availability (Gordon and Polle 2007). This allows their highly efficient cultivation in engineered systems called photobioreactors. They can also combine the ability for highly efficient growth with the biosynthesis and storage of various metabolites of commercial value. Indeed, diatoms have been produced at industrial scales for (i) use as live feed in hatcheries and (ii) production of the pigment fucoxanthin.

Diatoms are also known for their high lipid content and industrially relevant fatty acid profiles. For example, diatoms are cultivated for utilization at hatcheries due to their high long-chain polyunsaturated fatty acids contents (LCPUFAs), as these nutrients are critical for the health larval growth of some of the aquatic organisms mass-produced at aquaculture farms. *Thalassiosira* species employed in the current study are known to synthesize these LCPUFAs at high levels and thus are among the diatoms that are industrially cultivated for use as feed (Milledge 2011; Gouveia et al. 2009). *Thalassiosira* species are also considered to be a good candidate for lipid production (D'Ippolito et al. 2015; Graham et al. 2012).

Diatoms also possess a variety of pigments for (i) capturing solar energy of various wavelength ranges under regular light availability and (ii) photoprotection of the photosynthetic apparatuses and quenching the free radicals that form at destructively excessive light intensities (Kuczynska, Jemiola-Rzeminska, and Strzalka 2015). When taken as a dietary supplement, these pigments also have antiaging properties and beneficial health effects against diseases in humans (Kuczynska, Jemiola-Rzeminska, and

Strzalka 2015). These bioactive effects have generated immense interest in the mass production of these pigments. One of these pigments that has reached industrial-scale production is fucoxanthin from the diatom *Phaeodactylum tricornutum* (Kanamoto et al. 2021).

One unique metabolite produced by the diatom species of *Cylotella* and *Thalassiosira* genera is chitin nanofibers. Another unique feature of this metabolite is that it gets extruded to the cell exterior right after synthesis. Chitin and its deacetylated derivative chitosan are biocompatible, biodegradable, and nontoxic. They also have antibacterial and anti-inflammatory properties. Based on these properties, they are produced for industrial applications in pharmaceutical, cosmetics, food, and beverage industries, generating a total market value of 5 billion USD.

The current market highly depends on waste shellfish as a chitin feedstock. Impurity being the main one, this dependence brings about several problems for the current market. The main reason for these problems is the position of chitin in shellfish. Chitin in these organisms is a part of a 3-D structure along with other organics, such as proteins, and inorganics, such as calcium carbonate. This positioning and the covalent bonds between chitin and protein molecules complicate the production process and reduce their efficiency. The main complication of the extraction and isolation process is that they require the exposure of the chitin raw material to extreme pH and temperature conditions. This exposure usually results in unwanted alterations in chitin physicochemical polymer properties. Even after these processes, limitations typically exist on the extent of chitin purity that can be obtained. Diatom chitin has the potential to offer solutions to all these problems because the diatom chitin is extracellular, and these microorganisms can be cultivated under fully controlled growth conditions.

This study primarily aims to determine the extent of this potential by first cultivating three diatom strains from the *Thalassiosira* genera according to a standard cultivation protocol and under standard process conditions of a bubble column photobioreactor and then analyzing their chitin productivities. As a secondary goal, it analyzes protein and lipid contents as well as fatty acid distributions to assess the multiple product generation potentials according to the biorefinery-based production principle and also the suitability of the biochemical profiles for use as live feed in the aquaculture industry.

CHAPTER 2

LITERATURE REVIEW

Diatoms are a subclass of microalgae and are distinguished from the other classes with their silicon cell walls (frustules). These single-celled microscopic organisms rapidly grow in suspension with inputs such as water, atmospheric CO_2, and light. Their aerial biomass production rates can highly exceed those of terrestrial plants, and their division rates can be well below 24 hours (Chisti 2007). They are also known to biosynthesize metabolites of commercial interest given the correct selection of species and cultivation conditions. For instance, certain species of diatoms are known to be prolific producers of polyunsaturated fatty acids and pigments with potential applications in the food, feed, and pharmaceutical industries (Zulu et al. 2018).

2.1. Microalgae Cultivation Systems

Microalgae are cultivated in open systems or closed photobioreactors. This section will present the technical details of these systems, and their advantages and disadvantages for commercial-scale production will be discussed.

2.1.1. Open Ponds

Open ponds are easy to operate and inexpensive to install. The raceway ponds (Figure 1) are one of the most preferred open systems. They are usually built with a depth of about 30 cm out of concrete or polypropylene (Chisti 2007). In these systems, paddlewheels constantly mix the algal suspensions to keep the cells suspended. Apart from the depth, the most critical design parameter for open ponds is the length/width ratio. When this parameter is too high, the cultures are not mixed well, and the growth can get mass transfer limited. The main disadvantage of open ponds is the lack of control they provide over the cultivation conditions. For example, since the suspensions are directly open to the atmospheric conditions, microbial contamination, significant evaporative water losses, and high cultivation temperature fluctuations can be critical issues. Due to

these reasons, the biomass concentration in these systems is lower than those of closed systems and usually lies between 0.1 and 0.5 g/L (Enzing et al. 2014).

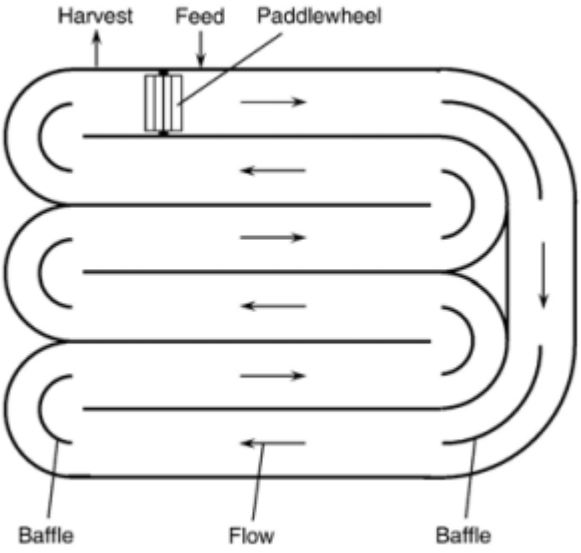

Figure 1. Schematics of raceway pond

Source: (Chisti 2007)

2.1.2 Closed Systems

Closed systems have been developed to eliminate the disadvantages of open systems (Chisti 2007). As the name implies, these systems cultivate the cells enclosed in transparent containers. Reactor geometry is the main variant between different types of closed systems. There are several important reasons why these systems are preferred over open systems: (i) evaporative water loss and microbial contamination risks are minimized, (ii) process conditions such as cultivation temperature, nutrient concentration, and pH can be controlled more efficiently, and (iii) in the case of its enrichment at the aeration gas CO_2 loss to the atmosphere can be reduced (Xiang et al. 2017). Closed PBRs usually have a higher surface area to volume ratio with respect to open ponds, which increases the light availability. Closed PBRs are operated in outdoor conditions with natural light and in indoor conditions with artificial light. Air or air enriched with CO_2 is constantly bubbled into the cultures for mixing and agitation, which increases mass transfer rate within the cultures (Chisti 2007). These improvements in turn increase the biomass production rates and biomass concentrations that can be obtained (Chisti 2007).

Higher initial and operational costs are the main disadvantages. Tubular, flat panel, and bubble column PBRs are the most frequently used closed systems.

Tubular Photobioreactors

In tubular PBRs algae are cultivated within tubes of diameters less than 10 cm. This constraint serves two purposes: it increases the surface area to volume ratio and improves mixing. Figure 2 presents the schematic of a typical system operated at outdoor conditions. Pumps are used to continuously flow the cultures in tubes at a velocity high enough to keep the cells in suspension. Tubes are usually placed in parallel to reduce overall land requirements. The lengths are usually kept below 30 meters to avoid CO_2 limitation and photooxidative damage (Chisti 2007). The cell suspensions are collected in vessels and aerated to replenish CO_2 and to remove excess O_2. These systems are used both in indoor and outdoor conditions.

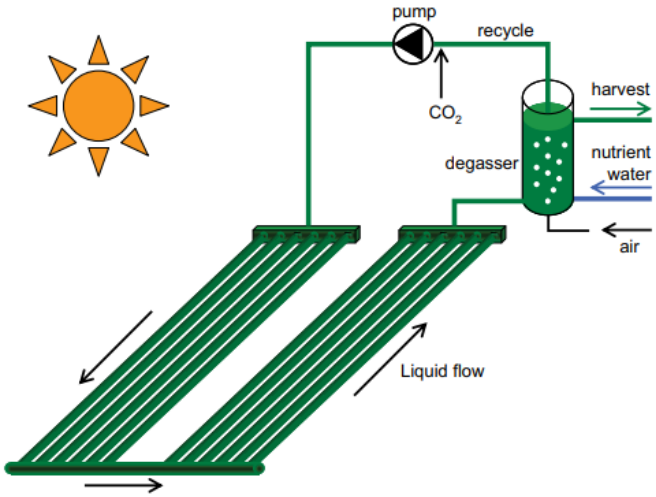

Figure 2. Schematic of a horizontal tubular PBR operated at outdoor conditions
Source: (Enzing et al. 2014)

Flat Panel Photobioreactors

In these systems, algae are cultivated in flat panels of depths less than 10 cm under constant mixing generated with airflow (Enzing et al. 2014). This threshold ensures the establishment of high surface area to volume ratios and increased light availability. Panels can be placed vertically relative to the ground or can be inclined to enhance light

availability, particularly for outdoor applications. The main advantage of these PBRs with respect to tubular systems is the absence of a concentration gradient.

Bubble Column Photobioreactor

In bubble column PBRs, the algae are cultivated in an aerated transparent vertical cylindrical vessel. This PBR type was selected for the current study due to a number of advantages it has for commercial-scale production with respect to other cultivation systems, such as high scalability, low space, and low energy input requirements (Gupta, Lee, and Choi 2015; Ugwu, Aoyagi, and Uchiyama 2008). These systems also provide high mass transfer rates without exposing the cells to high shear rates. They can deliver productivities that are similar to those obtained with tubular systems (Barahoei, Sadegh, and Afsharzadeh 2020).

2.2. Microalgae-Based Metabolites of Commercial Interest

Microalgae biosynthesize and store metabolites that have potential and real-life applications in the industrial-scale production of energy, health supplements, and animal feed (Figure 3). For instance, the pigments they use to capture solar energy are produced commercially for their beneficial health effects. The lipids they produce for energy storage can constitute more than 50% of their dry weight, making microalgae good candidates for producing biofuel feedstock material. A significant portion of these lipids is made of polyunsaturated fatty acids (PUFAs) that are commercially produced from other microorganisms and incorporated into health supplements. Furthermore, certain microalgal species are cultivated routinely in aquaculture as feed, owing to their high nutritional value (Bozarth, Maier, and Zauner 2009).

Microalgae have an exceptionally high growth rate and lipid content. Given the correct selection of growth conditions, they can double their biomass in a single day and simultaneously biosynthesize lipids amounting to more than 50% of their dry weight (Chisti 2007). To put these productivities into perspective, Chisti calculated the area requirements of various biodiesel sources to produce half of the United States transport fuel consumption in 2007 and concluded that while the best performing oil crop required an area equivalent to 24% of U.S. cropping area with microalgae this number could be

reduced down to less than 3% (Chisti 2007). Based on these properties, they have attracted significant research interest and have been studied as an alternative source of biodiesel (Khan, Shin, and Kim 2018).

From the commercial-scale production point of view, economics is the major drawback of algal biodiesel compared with other bio and fossil-based alternatives. This issue stems from both the high production cost of algal lipids and the low commercial value of biodiesel. High production costs are mainly attributed to the highly unique production processes involved and their low technological maturity as well as lack of economy of scale. Biofuel is also one of the lowest-value products that can be generated from algal biomass, with an estimated market value of 0.30 Euro/kg in 2022 (Zhou et al. 2022).

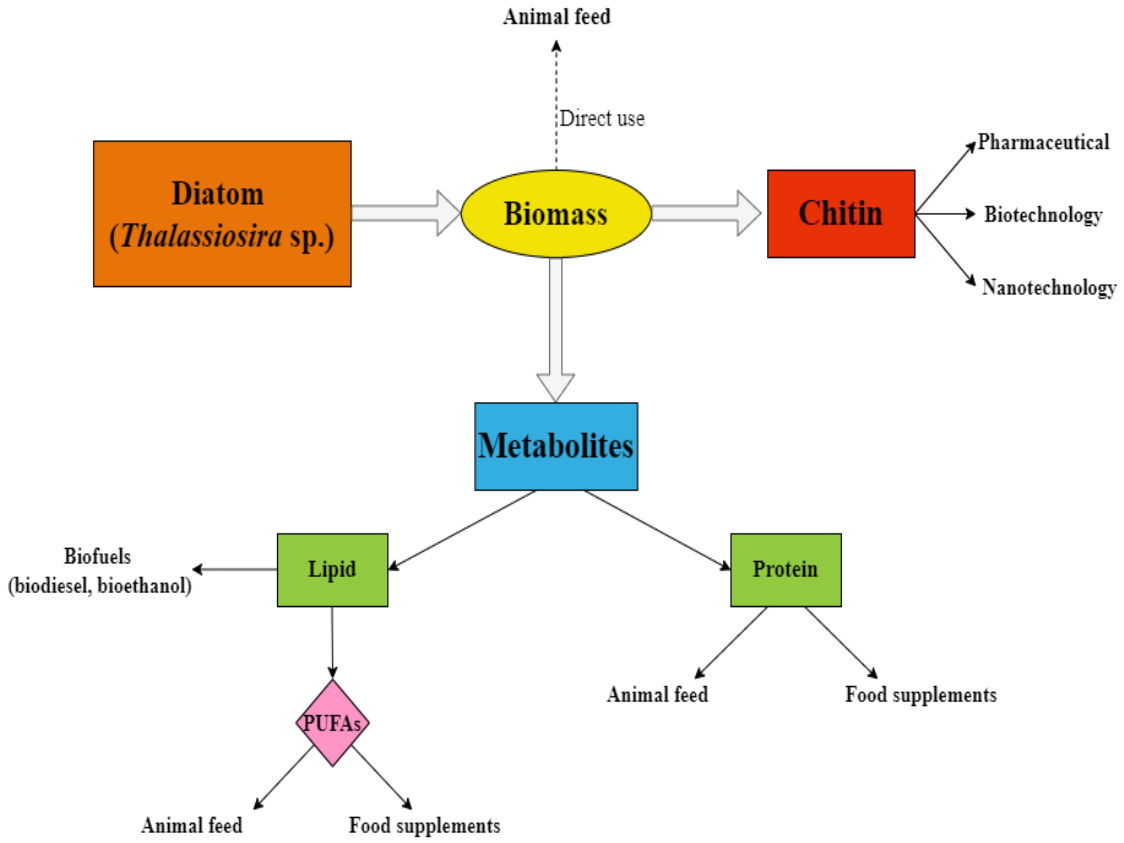

Figure 3. Current and potential applications of diatoms based biotechnology

The algal biorefinery concept emerged to improve the economic viability. The ultimate aim of biorefining is the complete utilization of algal biomass to generate multiple products of a range of commercial value. In this regard, screening algae for co-production of multiple industrially relevant products is of utmost importance. The species and strains that belong to the *Thalassiosira* genus are highly promising, considering their

known ability for the simultaneous biosynthesis of chitin nanofibers, polyunsaturated fatty acids, lipids, and proteins (Figure 3).

Polyunsaturated fatty acids, particularly eicosapentaenoic (EPA, 20:5n-3) and docosahexaenoic (DHA, 22:6n-3) fatty acids, are critical for human health as their availability in the body are well documented to be linked with the mitigation of pathological conditions and healthy development (Tocher et al. 2019). Humans cannot synthesize sufficient amounts of PUFAs for physiological needs, and thus their dietary intake is an absolute requirement (Ruiz-Lopez et al. 2015). Traditionally, marine fish has been the source of this nutrient in the human diet, but their actual input to the food web is by marine microalgae (Gouveia et al. 2009).

The current estimations clearly point out to a global deficiency of PUFA availability when the supply from the existing traditional sources and the cumulative amount required for healthy metabolic functioning of the human population are compared (Tocher et al. 2019). This deficiency has increased the interest for the study and use of alternative sources (Tocher et al. 2019). One such current commercial source is PUFA-rich heterotrophic microalgae, particularly those belonging to *Schizochytrium* and *Crypthecodinium* genera (Tocher et al. 2019). Microalgae-based PUFAs can also have price and palatability advantages over those from fish (Belarbi, Molina, and Chisti 2000; T. Lebeau and Robert 2003a).

Select species and strains of diatoms can also be prolific producers of EPA and DHA (Bozarth, Maier, and Zauner 2009; Zulu et al. 2018). Indeed, previous extensive industry-based research concluded that diatom species were among those that were of commercial potential for exploitation (Cohen and Ratledge 2005). Table 1 summarizes the lipid and EPA content of microalgae species. For instance, *Phaeodactylum tricornutum* is one of the species that has been frequently studied for PUFA production maximization through bioprocess engineering principles and genetic modification (Khan, Shin, and Kim 2018).

Table 1. Lipid and omega-3 fatty acid contents of microalgae

Microalgae	**Lipid content (%dw)**	**Omega -3 fatty acids (%dw)**	**EPA content (%dw)**	**References**
Botryococcus braunii	25-75			(Chisti 2007)
Chlorella sp.	28-32			(Chisti 2007)
Crypthecodinium cohnii	20			(Chisti 2007)
Crypthecodinium cohnii	30	9		(Barclay, Meager, and Abril 1994)
Cylindrotheca sp.	16-37			(Chisti 2007)
Dunaliella primolecta	23			(Chisti 2007)
Isochrysis sp.	25-33			(Chisti 2007)
Monallanthus salina	>20			(Chisti 2007)
Nannochloris sp.	20-35			(Chisti 2007)
Nannochloropsis sp.	31-68			(Chisti 2007)
Neochloris oleoabundans	35-54			(Chisti 2007)
Nitzschia sp.	45-47			(Chisti 2007)
	50	2.3		(Barclay, Meager, and Abril 1994)
Nitzschia conspicia			1.9-4.7 6.1	(T. Lebeau and Robert 2003a) (Chu, Phang, and Goh 1994)
Nitzschia leavis			2.59-2.76 1.41	(T. Lebeau and Robert 2003a) (Wen and Chen 2000)
Phaeodactylum tricornutum	20-30		2.2-3.9 2.2	(Chisti 2007) (Cerón Garcí et al. 2000)
Schizochytrium sp.	50-77	10		(Chisti 2007)
Schizochytrium sp.	33	10		(Barclay, Meager, and Abril 1994)
Tetraselmis sueica	15-23			(Chisti 2007)

Microalgae have been used as a feed source for the industrial production of aquatic organisms such as bivalves, crustaceans, and fish. In 2009, 30% of microalgae cultivated was utilized for this purpose (Gouveia et al. 2009). These microorganisms can be fed directly to the cultivated organisms or to their prey (Lucas, Southgate, and Tucker 2019). Diatoms have been cultivated in outdoor conditions at industrial scale for use as live feed in aquaculture farms and hatcheries that produce shrimps and bivalve mollusks (Table 2)

(Thierry Lebeau and Robert 2003). Biochemical profile and physical properties determine the applicability. The ideal diatom cell used in a hatchery should have (i) sufficient levels of EPA and DHA because their dietary presence is critical for the survival and enhanced growth of the organisms fed, and (ii) size and geometry fit for first ingestion and then digestion. Diatoms including *Thalassiosira pseudonan*a, *Skeletonema costatum*, and *Monochrysis lutheri* species are used commercially for aquaculture fish feed (Lavens and Sorgeloos 1996). Table 2 shows the diatom genera used in aquaculture and the organisms they are fed to. Species belonging to *Thalassiosira* genus, which are also studied in the current work, are cultivated as live feed for bivalve mollusk and penaeid shrimp (Lavens and Sorgeloos 1996).

Table 2. Diatom genera are used in the aquaculture feed industry

Source: (Lavens and Sorgeloos 1996)

Diatom Genera	**Applications**
Actinocyclus	BP
Bellerochea	BP
Chaetoceros	BL, BP, BS, PL
Cyclotella	BS
Cylindrotheca	PL
Nitzchia	BS
Phaeodactylum	BL, BP, BS, ML, PL
Skeletonema	BL, BP, PL
Thalassiosira	BL, BP, PL

BL: bivalve mollusk larvae, BP: bivalve mollusk postlarvae, BS: brine shrimp (Artemia), ML: freshwater prawn larvae, PL: penaeid shrimp larvae

Protein is another nutrient associated with issues both on the production and the consumption sides (Ewy et al. 2022; Geada et al. 2021). High environmental footprint and low areal yield of the conventional protein sources are the issues that need urgent solutions (Geada et al. 2021). There are two major issues on the consumption side: (i) the adverse health effects of over-reliance on animal-based food products and (ii) the limited presence of essential amino acids in conventional plant-based sources (Ewy et al. 2022). These issues motivate the search for alternative protein sources.

Chlorella and *Spirulina* species are cultivated industrially as a protein source for their advantages with respect to the current conventional sources (Geada et al. 2021; Khan, Shin, and Kim 2018). These algae can synthesize all the essential amino acids, and their cultivation under correct growth conditions can generate a biomass protein content of up to 70%, which is higher than the rest of the animal-based protein sources (Geada et al. 2021; Soni, Sudhakar, and Rana 2017). Furthermore, this cultivation can be sustained without arable land and freshwater. Algae-based protein is considered to be a more environmentally friendly alternative with respect to animal-based sources (Geada et al. 2021). Indeed, the life cycle assessments indicate that per kg of protein generated, algae's environmental footprint is lower than that of milk (Ye et al. 2018).

The current industrial and academic research on algae-based protein production focus on green algae and cyanobacteria strains (Koyande et al. 2019). Diatom species usually are not included in studies concerning the bulk production of proteins. However, at a diatom-based biorefinery, proteins can be one of the multiple products generated to diversify the revenue streams and maximize profitability.

2.3. Chitin and Chitin Derivatives from Diatoms

Chitin is a biopolymer of N-acetyl-glucosamine. It is biodegradable, biocompatible, and non-toxic (Figure 4). Chitin and its derivatives glucosamine and chitosan have a variety of applications in the biomedical, pharmaceutical, cosmetics, and food industries and create a cumulative market of 8.6 billion USD per year. The unit price of chitin varies with the quality and can go up to 200 USD per kg.

Chitin is found in the exoskeleton of crustaceans, such as crabs and shrimps, and also in fungal cell walls, and insects. Today, crustacean waste is the main source of chitin. In crustacean exoskeletons, chitin is tightly bound to proteins and minerals. Thus, chitin harvesting and isolation require multiple washes at alkaline and acidic conditions at high temperatures for demineralization and deproteinization (Rao, 2000). These harsh conditions modify the polymer structure of the chitin.

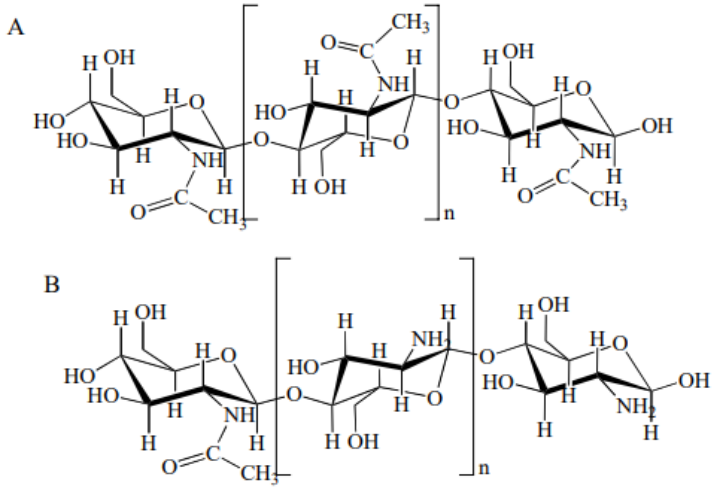

Figure 4. Chemical formula of chitin and chitosan

Source: (Aranaz et al. 2009)

Diatoms synthesize chitin nanofibers and extrude them from ports called fultoportulae lining the rim of their valves. The reason for the synthesis and extrusion is not clearly figured out. The most cited reason is that these fibers increase cell buoyancy, and this effect is needed to counteract the excessive settling force the cells experience due to heavy frustules (Gooday et al. 1985; Morin, Smucker, and Herth 1986). The basis for this assertion was experiments conducted that showed an increase in cell sedimentation rate following chitin biosynthesis inhibition (Gooday et al. 1985; Morin, Smucker, and Herth 1986).

Diatoms belonging to *Thalassiosira* and *Cyclotella* genera can produce high purity chitin nanofibers. However, until now, the studies that targeted the productivity analysis were based on the performance of a single strain *Cyclotella cryptica* (UTEX #1269). The productivities of *Thalassiosira* species and strains are unknown. Ozkan and Rorrer investigated the biomass, chitin, and lipid productivity of *C. cyrptica* by cultivating the strain at different photosynthetic light intensities (35, 70, 220, 370, and 520 $\mu E/m^2$-s) under photobioreactor conditions (Ozkan and Rorrer 2017c). They concluded that an inverse relationship existed between the final biomass and lipid concentrations, but the final chitin concentration was indifferent to light availability. However, the production rate of both metabolites and biomass decreased with decreasing average incident light intensity.

In another study, Ozkan and Rorrer investigated the effects of CO_2 availability on biomass, chitin, and lipid productivities by cultivating the diatom cells under varying inlet

pCO_2 concentrations of 200, 800, 2000, and 3000 ppm (Ozkan and Rorrer 2017a). Results were parallel to those obtained with the study on light availability mentioned above. They concluded that the final biomass and lipid concentrations and their production rate increased with increasing CO_2 availability until saturation was reached at pCO_2 of 2000 ppm. The chitin production differed by the generation of similar final concentrations regardless of the variation in pCO_2, but the production rates increased with increasing availability until the pCO_2 threshold at 2000 ppm.

Ozkan and Rorrer cultivated the same diatom strain in a bubble column PBR in fed-batch growth mode generating constant availability of CO_2, silicon, and nitrate in cultivation media (Ozkan and Rorrer 2017b). This growth mode increased both the final chitin concentration and its average production rate and resulted in values of 700 mg/L and 45 mg/L-day, respectively. This study also showed that chitin nanofiber biosynthesis was tied to cell division.

Chiriboga and Rorrer investigated the effects of silicon and nitrate delivery on chitin production under batch and perfusion-based growth conditions (O. G. Chiriboga and Rorrer 2017; O. Chiriboga and Rorrer 2018). Their studies showed that when the nitrate and silicon were perfused to cultures cultivated under their limitation, the perfusion rate proportionally controlled the chitin synthesis rate. They had also reported an increase in cell number density, chitin produced per cell, and chitin production rate when the nitrate/silicon ratio in the nutrient solution was increased from a ratio of 0.8 up to about 6.0 (O. Chiriboga and Rorrer 2018).

Xiang *et al.* carried out the techno-economic analysis of glucosamine and lipid production from the cultivation of the diatom *Cyclotella* sp. in a closed photobioreactor (PBR) and raceway open pond (RWP) systems (Xiang et al. 2017). The selling price of glucosamine was $35/kg, $82/kg, and $106/kg for RWP, PBR-high chitin concentration, and PBR-low chitin concentration scenarios, respectively. These values were more than the price of glucosamine ($20/kg) obtained from shellfish. Volumetric chitin productivity and final chitin concentration were the primary parameters that controlled the production cost of glucosamine. For example, when the productivity was doubled with respect to the base case scenario, the glucosamine selling price could be reduced by about 40%.

CHAPTER 3

MATERIALS AND METHODS

3.1. Selection of Diatom Strains for Chitin Production Experiments

Strains known to be chitin producers were included in the current study. Strains belonging to the two major species of the *Thalassiosira* genus were selected to ensure the analysis of possible species-specific differences (Table 3.).

Table 3. Information on the strains included in the current study

Strain number	**Strain name**	**Abbreviation**	**Original Habitat**
1336	*Thalassiosira weissflogii*	TW-1336*	Marine
122.79	*Thalassiosira pseudonana*	TP-122.79**	Marine
2135	*Thalassiosira pseudonana*	TP-2135**	Marine

*CCMP: Bigelow National Center for Marine Algae and Microbiota, Maine, U.S.A
**SAG: Culture Collection of Algae, Göttingen Germany

3.2. Cultivation of the Inocula for the Photobioreactor Experiments

The inocula for the photobioreactor experiments were cultivated axenically in flasks of 500 mL volume. Harrison's artificial seawater medium with elevated concentrations of nitrate, phosphate, and silicon -5.32 mM, 0.24 mM, and 0.50 mM, respectively- was utilized. The cultures were subcultured in a laminar flow cabin and were kept at the log-phase of growth. The medium and the flasks were autoclaved prior to subculturing to ensure the establishment of axenic conditions. The inoculated flasks were placed in an illuminated and temperature-controlled incubator under process conditions summarized in Table 4. The incident photosynthetically active radiation (PAR) intensity to the flask surfaces was measured with a PAR sensor and adjusted to about 100 μE/m2-second. The temperature was set to 20^{o}C. The flasks were mixed manually once each day for 10 seconds.

Table 4. Process conditions for flask cultures

Process parameter	**Value**	**Units**
Cultivation temperature	20	℃
Culture volume	150	mL
Average incident light intensity	100	µm/m^2-s
Light:dark period	14:10	hour:hour
Initial nitrate concentration	5.32	mM
Initial phosphate concentration	0.24	mM
Initial Si concentration	0.5	mM

3.3. PBR Design and Characterization

A bubble column photobioreactor was used to cultivate the strains under fully controlled process conditions (Figure 5). This reactor type was selected due to properties including ease of scale-up, low operational energy input requirement, which are all deemed critical for commercial scale production.

Figure 5. Bubble column photobioreactor

The PBR was fully autoclavable and leak-proof to ensure contamination free unialgal growth. It consisted of a cyclindrical glass vessel (with 13 cm diameter and 44 cm height) placed between stainless steel top and bottom plates. The top plate housed the

sealed connections for the sampling line, temperature measurements port, nutrient inlet, exhaust gas outlet as well as the heat exchanger coil inlet and outlet. The cultivation temperature was set to 20℃ by pumping temperature-controlled water through this coil. Aeration gas line was connected to the bottom plate.

3.3.1. Aeration System

The diatom suspensions were aerated during cultivation to ensure the availability of CO_2 and the removal of excess dissolved oxygen. Two mass flow controllers were used to increase the CO_2 content of the aeration gas to 1% (volume/volume) and to generate a total flow rate of 2 L/min. The gas flow was (i) sterilized using 0.22µm pore sized HEPA filter, (ii) humidified by passing through sterile water, and (iii) introduced to the cultures through four holes of 1 mm diameter located at the center of the bottom plate. Mass transfer coefficient (k_{La}) of the aeration system was measured at five aeration flow rates using Van't Riet's method for characterization. A k_{La} value of 12.5±0.3 hr^{-1} was measured at a flow rate of 2 L/min.

3.3.2. Lighting System

The lighting system consisted of (i) four vertical column of light bulbs each housing five-halogen light bulbs and (ii) a dimmer switch that controls the light intensity output of the bulbs. These columns were placed orthogonal to the reactor surface at a distance of 10 cm. The dimmer position-average incident light intensity relation was calibrated by measuring the PAR intensities at the inner surface of the vessel using a PAR sensor at 1.25 cm interval at five dimmer settings. Average PAR intensities of up to 570 µmol/m^2-sec could be sustained with the system.

3.3.3. Temperature Control System

The temperature control system consisted of (i) a heat exchanger coil and a temperature measurement port immersed into the cultivation vessel, and (ii) a refrigerated circulator. Inlet and outlet of the coil and the port were placed on the reactor top plate and were all leak-tight. The temperature of the suspensions was constantly monitored with a

thermocouple inserted into the port. The circulator's temperature was adjusted based on the thermocouple readings. A constant temperature of 20℃ was maintained during cultivation.

3.4. Two-stage Photobioreactor Cultivation Process

The diatom strains were cultivated according to a two-stage protocol. The first stage aimed the acclimation of the flask cultures to the reactor conditions and cell synchronization. The second stage targeted the productivity analyses of all the metabolites of interest under first silicon replete and following its exhaustion under silicon deplete conditions. Nitrate availability was ensured during both stages as this was an absolute requirement for chitin biosynthesis according to previous studies (Ozkan and Rorrer 2017c, 2017a, 2017b; O. Chiriboga and Rorrer 2018).

Flask cultures were washed with fresh nutrient medium and then transferred to the reactors to initiate the first stages at a cell number density of about $1.0x10^5$ cells/mL. The initial suspension volume was 3.8 L. The initial dissolved silicon and nitrate concentrations were 0.5 mM, and 5.32 mM, respectively. The average incident light intensity was set to 50 μmol/m^2-second. Daily samples were taken from the reactor and assayed for optical density at 750 nm (OD 750). Dissolved silicon and nitrate concentrations were measured using spectrophotometric methods. The first stage ended 48 hours after the silicon depletion.

The second stage commenced with the pulse addition of sufficient volume of silicon stock solution (500 mM in $Na_2SiO_3.9H_2O$ form) to the suspensions to generate a concentration of 1 mM. The average incident light intensity was increased to 250 μm/m^2-second. The reactor was sampled for cell number density, biomass, chitin, lipid and protein analyses. Soluble silicon and nitrate were also measured daily with the aforementioned methods.

During the 2^{nd} stage, a total of 4 mM silicon was delivered to the suspensions with four equivalent pulse additions. The timing was set according to results from the daily nutrient concentration measurements: appropriate volume of stock solution was pulsed when the dissolved concentration fell below 0.5 mM. The reason for multistep addition was the limited solubility of this nutrient in seawater, amounting to about 1.5 mM. The total dosage was selected to ensure the generation of measurable amounts of biomass and

metabolite concentrations. Similarly, when the measured nitrate concentrations went below 2 mM, sterile 1 M nitrate stock was added to the suspensions in pulse to increase the concentration to 5 mM. The cumulative volume of all these additions were less than 1.5% of that of the diatom suspensions and thus the resultant volume changes were ignored in the productivity calculations. The second stage ended when the cell number density reaches a plateau. The suspensions remaining in the reactor were processed for chitin nanofiber isolation.

3.4.1. Cell Number Density

Hemocytometer method was used to determine cell number densities. Daily samples were injected into the hemocytometer chamber and images were taken across the entire area using a light microscope (Olympus, CX31). The images were processed using ImageJ image analysis software. The cell number densities (N_{cell}) were calculated using the following relation:

$$N_{cell} = \frac{n_{count}}{A_i \times D_h} \tag{3.1}$$

where n_{count} is the number cells counted in the image, A_i is the imaged area (equal to $1.43 \cdot 10^6$ μm^2 when 10X objective is used), and D_h is the hemocytometer depth (200μm).

3.4.2. Biomass Concentration Analysis

Biomass concentration was measured as ash free dry weight. Diatom suspensions were harvested with centrifugation at 3000 g for 10 minutes. The pellets were washed with 35 g/L NaCl solution once and were dried at 80°C until constant weight. Ash free dry weight was found by combustion of the samples in a muffle oven (Magma Therm, MT Series) at 550 °C for 8 hours. The biomass concentration ($X_{biomass}$) was defined as:

$$X_{biomass} = \frac{m_{dry} \times F_{AF}}{V_{sample}} \tag{3.2}$$

where V_{sample} is the volume of the sample harvested (L), m_{dry} is the mass of the sample after dried at 80°C, F_{AF} is the organic content of the dry biomass:

$$F_{AF} = \frac{m_i - m_f}{m_i} \quad (3.3)$$

where m_i and m_f are the mass of the samples before and after combustion, respectively.

3.4.3. Dissolved Silicon Concentration

The dissolved silicon concentration of diatom suspensions was measured daily according to Fanning and Pilson's method (Fanning and Pilson 1973). Photobioreactor samples were first centrifuged at 3000 g for 10 minutes to separate the cells from the nutrient medium. Then 0.1 mL of 8 M HCl solution and 0.2 mL of 115 mM ammonium molybdate solution were added to 5 mL of supernatant. After 10 minutes, the optical density of solutions was measured at a wavelength of 360 nm using a UV-VIS spectrophotometer (Shimadzu, UV 2600). For calibration purposes, a number of standards were prepared with sodium metasilicate (Na_2SiO_3) and were analyzed along with the diatom samples.

3.4.4 Dissolved Nitrate Concentration

The dissolved nitrate concentration of the reactor samples was measured daily using a spectrophotometric method (Collos et al. 1999). First, centrifugal supernatants were diluted with deionized water to ensure that the concentrations would fall into the linear range of the method. Then, the optical density of the diluted samples was measured at 220 nm wavelength using a UV-VIS spectrophotometer and a 1 cm quartz cuvette. Samples with nitrate concentrations of 5.00 mM, 2.50 mM, 1.25 mM, 0.63 mM, and 0.31 mM were analyzed along with the reactor samples for calibration. Soluble nitrate analysis and continuous nitrate availability were critical for the current study as chitin biosynthesis is known to stop when cells are cultivated under its limitation (Ozkan and Rorrer 2017a, 2017c, 2017b).

3.4.5 Optical Density of Diatom Suspensions

The changes in cell number density were also assessed by daily optical density analyses that were made at wavelengths of 530 nm, 680 nm, and 750 nm using a 1 cm

cuvette (Appendix A1). When the measured values exceeded 1.0, the samples were diluted with the associated centrifugal supernatants to ensure a linear response.

3.4.6 Total Lipid and Fatty Acids

The biomass lipid content was determined with the modified Folch method (Ozkan and Rorrer 2017c, 2017b). The lipids were extracted from dried biomass with chloroform:methanol (2:1 v/v) solution for 12 hours. The extracts were washed first with 0.88% KCl aqueous solution and then with methanol:H_2O (1:1, v/v). At each of these washes, (i) the extracts loaded with the solutions were vortexed for 1 minute, (ii) the obtained solutions were centrifuged at 1000 g for 10 minutes for phase separation, and (iii) the upper phases containing the impurities were discarded. The mass of the extracted lipids was measured gravimetrically. For that, the washed extracts were pipetted to preweighed vials using glass Pasteur pipettes, and the solvents were evaporated under N_2 flow.

The fatty acid profiles of the strains were determined at samples taken during the stationary growth phase. The lipids were transesterified with the boron trifluoride-methanol method (Metcalfe, Schmitz, and Pelka 1966). The solvent layers containing the fatty acid methyl esters were injected to a gas chromatograph (Agilent, 112-88A7E) equipped with a flame ionization detector and HP-88 column (100.0 m x 250 μm x 0.20 μm). The injector temperature was 250^oC. The column temperature was kept at 140^oC for 5 minutes, increased to 240^oC in 15 minutes, and held at this temperature for 40 minutes. Helium was used as the carrier gas at 1.3 mL/min flow rate.

3.4.7 Total Protein

The protein content of the diatom biomass was determined with the Bradford method (Bradford 1976). This method consisted of two consecutive steps: hydrolysis and spectrophotometric analysis. For hydrolysis, 2 mL of 0.5 M NaOH solution was added to wet biomass pellets obtained by centrifugation at 16,000 g for 10 minutes. The suspension temperature was maintained at 80^oC for a total of 20 minutes. The hydrolysates solid and liquid phases were separated by centrifugation (16,000 g for 30 minutes) after the first 10 minutes. One mL of nanopure water was added to the supernatants, and the solids were

re-hydrolyzed under the same process conditions. The solid and liquid phases were separated centrifugally after the second hydrolysis. The supernatants from both steps were combined. The protein-dye complexes were generated by adding 0.1 mL of the hydrolysates to 5 mL of reagent containing 100 mg Coomassie Brilliant Blue (G-205), 50 mL 95% pure ethanol, and 100 ml 37.5% phosphoric acid diluted with (a total volume of 1 L) distilled water. The optical density of the samples were measured at a wavelength of 595 nm after 30 minutes. Bovine serum albumin solutions of known concentration were assayed along with the hydrolysates for calibration.

3.5 Chitin Nanofiber Analyses

Chitin nanofiber concentration (C_{Chitin}, mg/L) of the samples was calculated by

$$C_{Chitin} = \frac{\rho_{chitin} \pi \, r^2 l_{total}}{V_{sample} D} \tag{3.4}$$

where ρ_{chitin} is the density of chitin nanofibers, equal to 1495 mg/cm^3 (Dweltz, Colvin, and McInnes 1968), r is the average radius of the fibers in cm, l_{total} is the total length of chitin nanofibers present in the sample analyzed in cm, V_{sample} is the sample volume in L and D is the sample dilution rate. As further described in the following sections, the fiber length and diameter estimations were based on the analyses of the images obtained with differential interference contrast and scanning electron microscopes, respectively.

3.5.1 Chitin Nanofiber Length Measurements

Length distributions of the nanofibers were determined daily during the second stage with an imaging-based method. Since the fibers are non-pigmented and transparent, the contrast between the fibers and the background had to be enhanced. This enhancement was achieved by utilizing a differential interference contrast filter and removing the water content of the samples through evaporative drying prior to imaging. A number of further measures were taken to ensure that the images would show fibers with clear beginnings and ends. First, samples were washed with nanopure water after centrifugation at 16,000 g for 30 minutes, keeping the sample volumes constant. The replacement of cultivation

media with nanopure water prevented the formation of salt crystals after drying. Washed samples were diluted to a constant cell number density through a series of dilutions, first with nanopure water and then at the last step with HPLC grade ethanol, resulting in a volume ratio of 1:1. The dilution helped to avoid crowding and entanglement of the fibers. The generation of the binary solvent mixture before drying minimized the coffee ring effect and ensured a more uniform deposition of the fibers during drying (Shi, Yang, and Bain 2019). Samples with a volume of 0.30 μL were pipetted onto pre-cleaned glass slides (Isolab, Superior quality glass slides) and dried at room temperature (21±2°C). The deposits formed after drying were imaged using a DIC microscope (Zeiss, Axio Observer Z1) equipped with a motorized stage and a 64X objective. The complete area of the deposits was scanned, and thus all the fibers originally present in the suspensions could be imaged. The images were analyzed for fiber length using ImageJ image analysis software. The results could be used to calculate the total chitin nanofiber length of the samples (l_{total}), considering that all the fibers deposited were first imaged and then analyzed for length. Only fibers with clear beginning and end were used for the length distribution analyses.

3.5.2 Chitin Nanofiber Diameter Measurements

The average fiber diameters (r) were determined at two samples taken during the second growth stage for each strain. These samples were taken 48 hours after the first and the last silicon dosages and characterized the log and the stationary phases of growth, respectively. The sample preparation protocol used for the length analyses was reused except for using aluminum foil as the drying surface. The samples were sputter coated with gold for 120 seconds at a pressure of $1 \cdot 10^{-1}$ mbar and imaged with a scanning electron microscope (Fei Quanta, 250 FEG). Fiber diameters were determined manually using ImageJ image analysis software.

CHAPTER 4

RESULTS AND DISCUSSION

4.1. Cell Number Density

As mentioned in the previous chapters, photobioreactor experiments were carried out in two stages. The first stage began with the transfer of diatom cultures cultivated in flasks to the reactor. This stage synchronized the cells and allowed them to adjust to photobioreactor process conditions. The second stages were started 48 hours after the dissolved silicon in the nutrient solution was depleted. Silicon concentrations were increased to 1 mM (by adding a sufficient volume of 200 mM sodium metasilicate stock solution) at the start of the 2^{nd} growth stages. Dissolved silicon concentration was measured daily, and when the measured values fell below 0.5 mM, the stock solution was dosed to increase the silicon concentration by one mM. This stepwise delivery ensured that the silicon solubility limit of 1.8 mM was not exceeded at all times (Ozkan and Rorrer 2017b). In total, four mM of silicon was delivered. The total dosage was selected to ensure the generation of (i) high enough biomass concentrations that allow the gravimetric analyses of metabolite contents and (ii) silicon depleted growth conditions towards the end of the cultivation. Constant nitrate availability was maintained during experiments through pulse additions of $NaNO_3$ stock solution (532 mM concentration) when the daily measured values were below one mM. Constant nitrogen availability was critical for understanding chitin productivity because nitrogen is a part of chitin's monomer, N-acetylglucosamine, and under its limitation the synthesis of this polymer is known to stop (Ozkan and Rorrer 2017c, 2017a, 2017b). Along with nitrate, phosphorus was also added to the medium with the same stock solution at a concentration of 24 mM, calculated according to the N/P ratio of the original medium recipe.

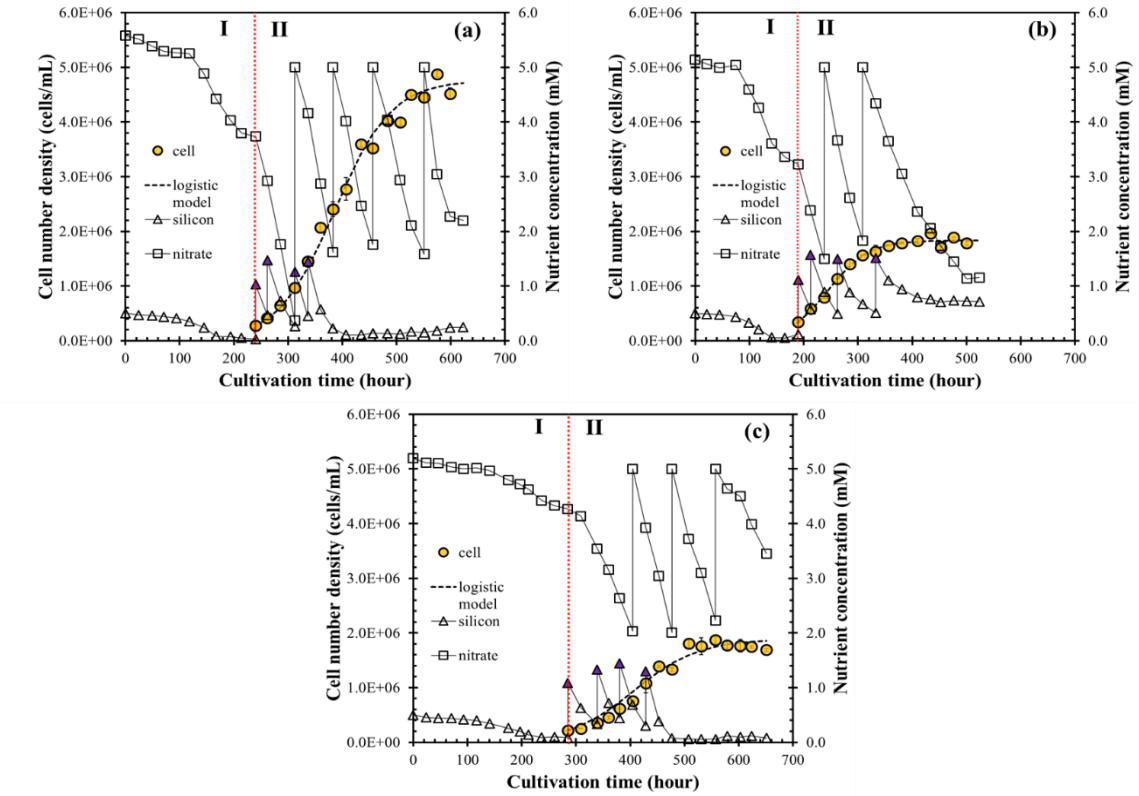

Figure 6. The changes in cell number density, dissolved nitrate, and silicon concentrations in suspension during photobioreactor cultivation for (a)*T. weissflogii* 1336, (b) *T. pseudonana* 122.79, and (c) *T. pseudonana* 2135 strains.

Figure 6 shows the changes in cell number density and nutrient concentration with respect to cultivation time for all the strains studied. The logistic model parameters, including cell production rate constants ($k_{P\text{-}cell}$), final cell number densities ($C_{f\text{-}cell}$), and peak production rates ($R_{P,\text{-}cell}$), are presented in Table 5. Except for the *T. pseudonana* 122.79, all the strains fully consumed the delivered silicon at the end of the cultivation. The final cell number density of *T.weissflogii* 1336, *T.pseudonana* 122.79, and *T.pseudonana* 2135 strains were $4.76 \cdot 10^6 \pm 1.0 \cdot 10^5$ cells/mL, $1.83 \cdot 10^6 \pm 2 \cdot 10^4$ cells/mL, and $1.89 \cdot 10^6 \pm 7 \cdot 10^4$ cells/mL, respectively (Table 5). *T.pseudonana* strains produced similar final cell number densities, while the final density with *T.weissflogii* was about 2.5 times that of the other strains. All the strains continued consuming significant amounts of nitrate even after the cell number density plateaus were reached. *T.pseudonana* 122.79 had the highest rate constant showing that this strain reached its final density earlier than the others. *T.weissflogii* strain had the highest peak cell production rate. The final cell yield on silicon was $4.7 \cdot 10^6$ cell/mM and 1.89 10^6 cell/mM for *T. weissflogii* 1336 and *T.pseudonana* 2135 strains, respectively. Such a large variability between the strains can

be an indication of the difference in cellular morphology between the strains, such as cell size or frustule thickness.

Table 5. Logistic model-based cell productivity parameters for Stage II cultivation of the *Thalassiosira* strains

Strains	$k_{P\text{-}cell}$ (h^{-1})	$C_{f\text{-}cell}$ (cell/mL)	$R_{P,cell}$ (cell/mL-day)
T. weissflogii 1336	$1.92\cdot10^{-2}\pm5.86\cdot10^{-4}$	$4.76\cdot10^{+6}\pm1.03\cdot10^{+5}$	$5.50\cdot10^{+5}\pm3.61\cdot10^{+2}$
T. pseudonana 122.79	$2.70\cdot10^{-2}\pm1.18\cdot10^{-3}$	$1.83\cdot10^{+6}\pm2.64\cdot10^{+4}$	$2.97\cdot10^{+5}\pm1.86\cdot10^{+2}$
T.pseudonana 2135	$1.68\cdot10^{-2}\pm9.92\cdot10^{-4}$	$1.89\cdot10^{+6}\pm7.01\cdot10^{+4}$	$1.91\cdot10^{+5}\pm4.17\cdot10^{+2}$

4.2. Biomass Concentration

Figure 7 shows the changes in biomass and dissolved nutrient concentrations of the *Thalassiosira* cultures during the second growth stage. The biomass concentration increased for about 80 hours after dissolved silicon depletion for *T. weissflogii* 1336 and *T. pseudonana* 2135 strains. The final biomass concentration ($C_{f\text{-}biomass}$) obtained with *T. weissflogii* 1336 was higher than the rest of the strains. However, *T. pseudonana* 122.79 had the highest production rate ($k_{P\text{-}biomass}$) and thus the peak biomass productivity ($R_{P,biomass}$) (Table 6). All strains biomass production rate constants were lower than the cell production rate constants. This discrepancy shows that the biomass production continued after the stationary phase cell number densities were reached.

There was a positive correlation between the final cell number densities and biomass concentrations obtained with the strains. For example, the final cell number density and final biomass concentration of *T. weissflogii* 1336 strain were the highest. However, the final biomass per cell value of *T. weissflogii* 1336 strain was about 574 pg/cell, which was about half of those of the other strains, 1169 pg/cell and 1069 pg/cell for the *T. pseudonana* 122.79 and 2135 strains, respectively.

Table 6. Logistic model-based biomass productivity parameters obtained with Stage II cultivation of the *Thalassiosira* strains.

Strains	$k_{P\text{-}biomass}$ (h^{-1})	$C_{f\text{-}biomass}$ (g/L)	$R_{P,biomass}$(g/L-day)
T. weissflogii 1336	$1.38\cdot10^{-2}\pm2.33\cdot10^{-4}$	2.73±0.03	$2.26\cdot10^{-1}\pm4.45\cdot10^{-5}$
T. pseudonana 122.79	$1.80\cdot10^{-2}\pm4.46\cdot10^{-4}$	2.14±0.03	$2.31\cdot10^{-1}\pm7.13\cdot10^{-5}$
T.pseudonana 2135	$1.33\cdot10^{-2}\pm2.77\cdot10^{-4}$	2.02±0.04	$1.61\cdot10^{-1}\pm47.07\cdot10^{-5}$

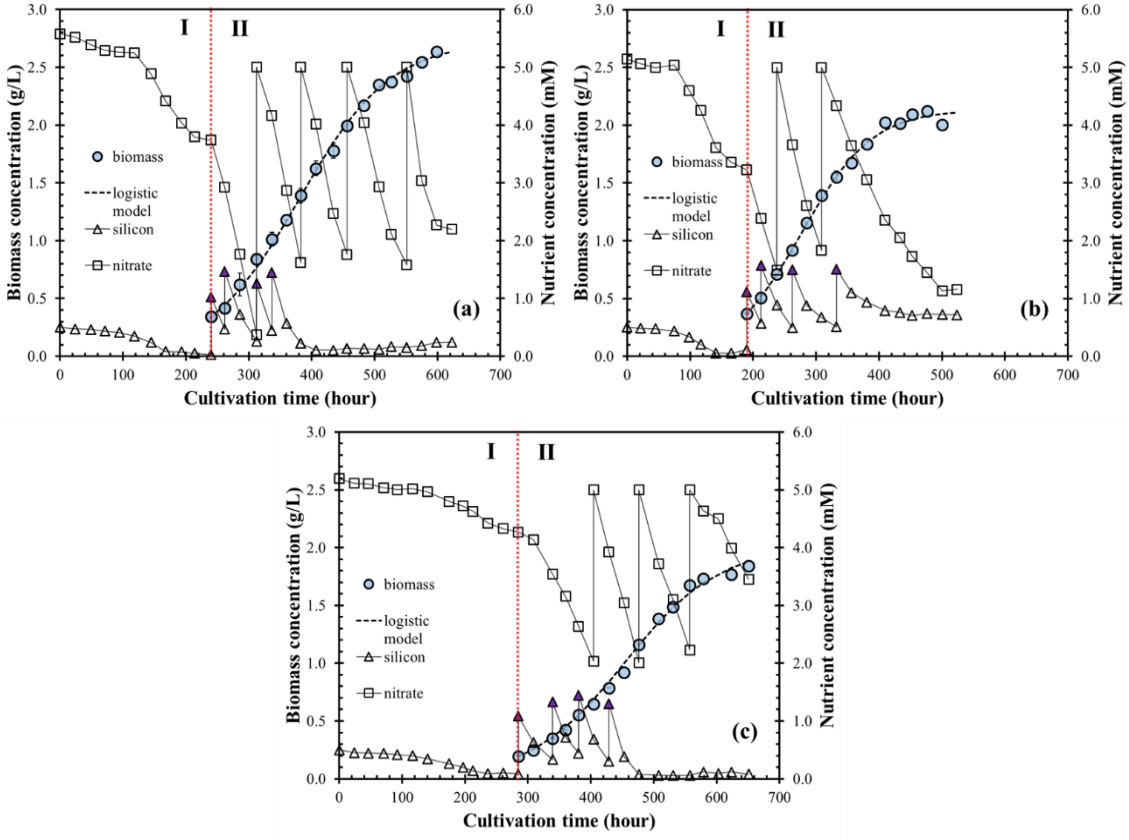

Figure 7. The changes in biomass and nutrient concentrations during photobioreactor cultivation for (a) *T. weissflogii* 1336, (b) *T. pseudonana* 122.79, and (c) *T. pseudonana* 2135 strains.

4.3. Chitin Productivity

Figure 8 shows the exemplary scanning electron microscope (SEM) images of the strains during log and stationary growth phases. The fibers produced by all the strains were straight and had a cylindrical shape. Fiber diameters were determined from the manual analysis of the images for log and stationary phases (Table 7). The average diameters (*r*) obtained with *T.weissflogii* 1336 and *T.pseudonana* 122.79 were similar and were about 70 nm. On average, *T. pseudonana* 2135 biosynthesized fibers of larger diameter than the other strains for both growth stages. The average diameters were 95.0±1.9 and 86.2±1.2 nm during log and stationary growth phases, respectively. LeDuff and Rorrer reported average fiber diameters of 56 nm for *C. cryptica* CCMP 332, cultivated in a bubble column photobioreactor (LeDuff and Rorrer 2019a).

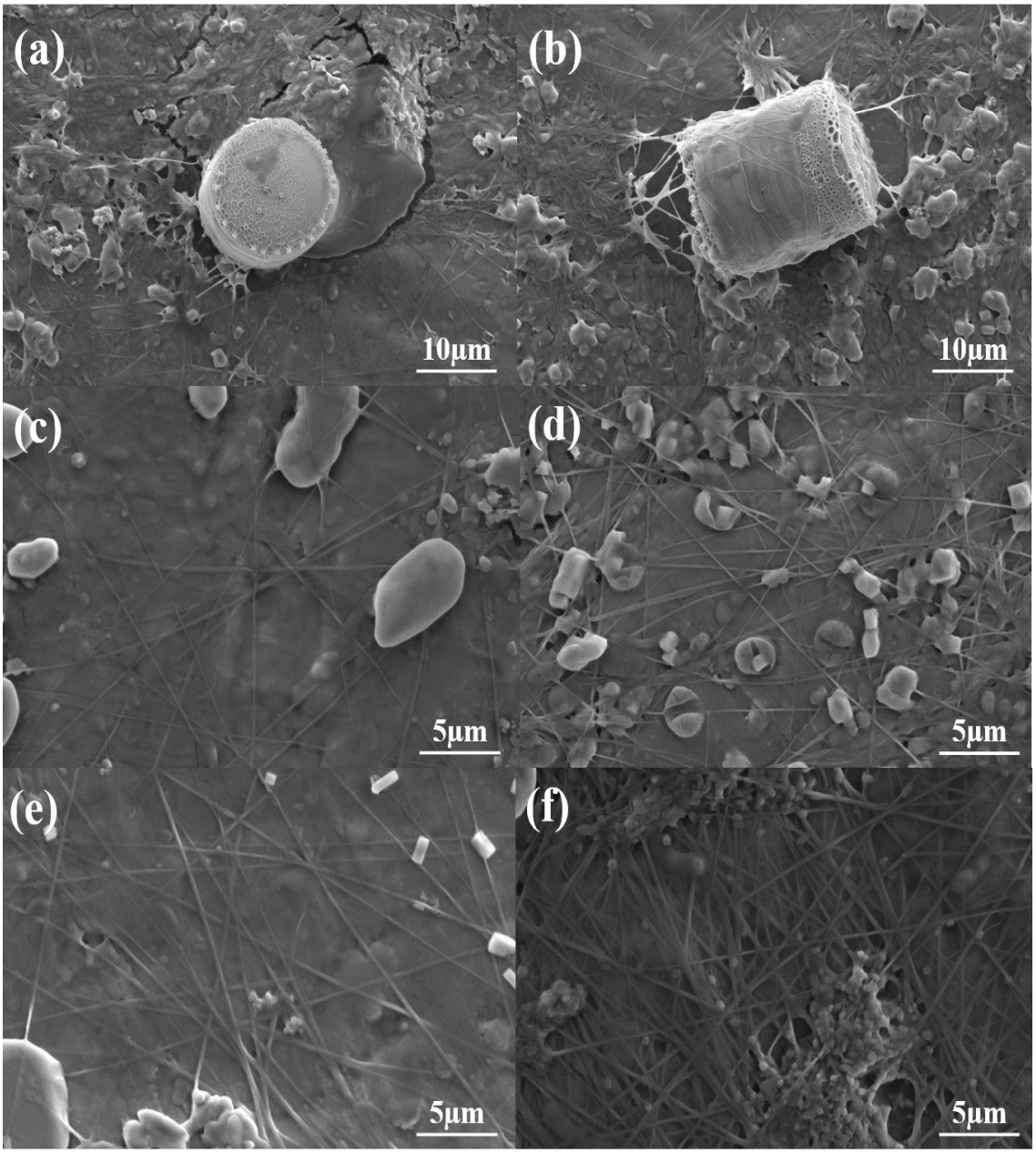

Figure 8. Exemplary SEM images of the strains (a, b) *T.weissflogii* 1336, log and stationary phases, respectively, (c,d) *T.pseudonana* 122.79, log and stationary phases, respectively, (e,f) *T.pseudonana* 2135, log and stationary phases, respectively.

Table 7. Diameter lengths of chitin nanofibers produced by strains of *Thalassiosira* genera in logarithmic and stationary growth phases. (1.0S.E. = ±1.0 standard error and n=number of measurements)

Strain	Growth phase	Average diameter (nm)	1.0 S.E.
T. weissflogii 1336	Log	69.7	2.1 (n=60)
	Stationary	69.2	0.9 (n=273)
T. pseudonana 122.79	Log	68.5	1.4 (n=159)
	Stationary	69.4	1.6 (n=171)
T.pseudonana 2135	Log	95.0	1.9 (n=132)
	Stationary	86.2	1.2 (n=248)

Figure 9 presents the variation of chitin concentrations in diatom suspensions during the second growth stage. The chitin productivity of *T. weissflogii* 1336 and *T. pseudonana* 2135 strains increased drastically following the silicon depletion in the liquid medium. LeDuff and Rorrer also reported chitin productivity increases under silicon-depleted growth conditions with *Cyclotella cryptica* CCMP 332 (LeDuff and Rorrer 2019b).

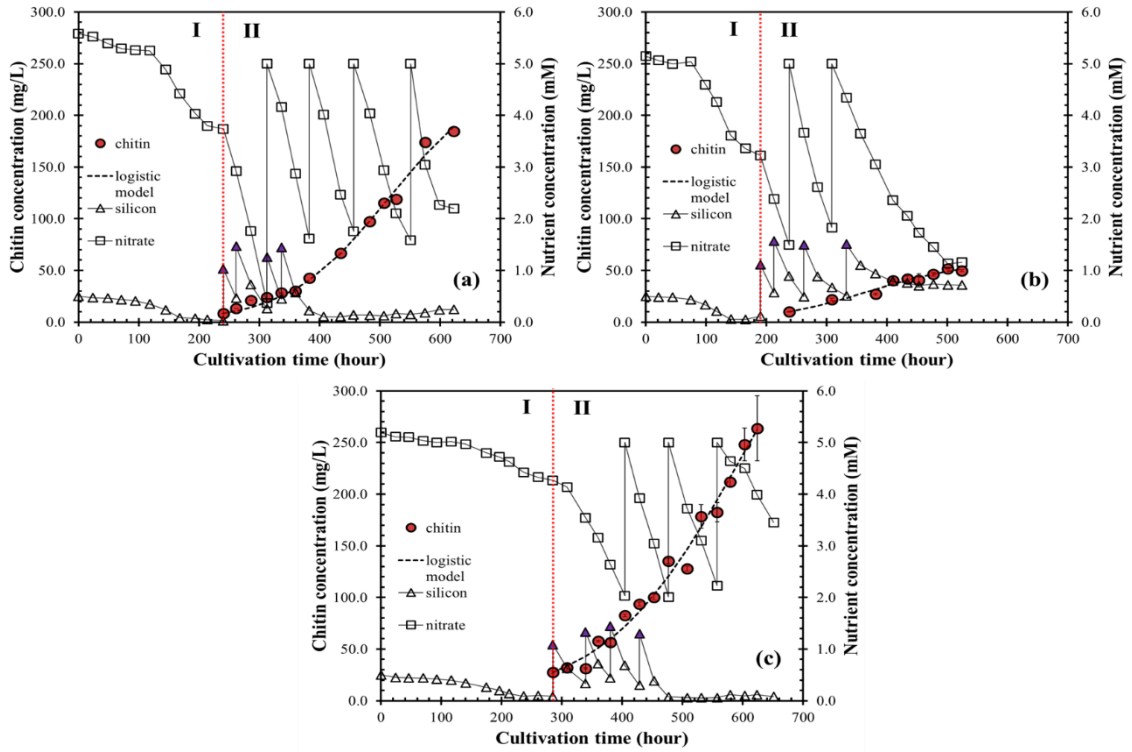

Figure 9. The changes in chitin and nutrient concentrations during photobioreactor cultivation for (a) *T. weissflogii* 1336, (b) *T. pseudonana* 122.79, and (c) *T. pseudonana* 2135 strains.

Figure 10 shows the chitin productivity parameters obtained with the logistic model. The final chitin concentrations ($C_{f\text{-}chitin}$) obtained with *T. weissflogii* 1336, *T. pseudonana* 122.79, and *T.pseudonana* 2135 strains were 241 mg/L, 59.1 mg/L, ve 460 mg/L, respectively. In parallel to $C_{f\text{-}chitin}$ *T. pseudonana* 2135 also had the highest peak production rate, even though its production rate constant ($k_{P\text{-}chitin}$) was the lowest. The production rate constants for chitin were lower than those of biomass for all the strains. This difference indicates that chitin production in diatoms may continue even when the biomass concentrations reach a plateau.

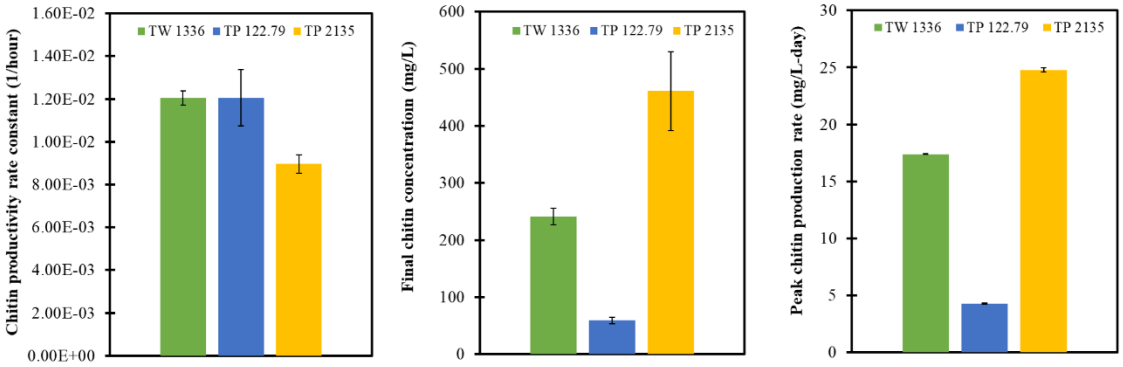

Figure 10. Logistic model-based chitin productivity parameters obtained with Stage II cultivation of the *Thalassiosira* strains (a) chitin productivity rate constant, (b) final chitin concentration, and (c) peak chitin production rate.

4.4. Biomass Lipid, Protein, and Chitin Contents

The results clearly indicate the critical role silicon availability plays in the biochemical profile of all the strains. The 1st growth stages were concluded after 48 hours of dissolved silicon exhaustion and the 2nd growth stages were started with a pulse silicon dosage sufficient to generate a concentration of 1 mM in the growth media. This sudden availability contrast provided a good opportunity for the analysis.

The protein content of the strains reached about 30% at the highest level (Figure 11). With *T.weissflogii* 1336 and *T.pseudonana* 2135 this level was reached 24 hours after the first silicon dosage. As the cultures progressed into Stage II, the protein contents decreased with all the strains. There was a clear inverse relation between the protein and lipid contents of *T.pseudonana* 2135 following 450th hour. This strain had the lowest protein content of about 9% at the end of Stage II but at the same time had the highest

lipid content of 45%. To put these ratios into perspective, the protein content of meat and dairy products usually ranges from about 30 to 40%. Thus, neglecting the productivities, the protein contents achieved in the current study suggest the suitability of these strains as an alternative protein source.

The results show that lipid contents exceeding 45% was possible under silicon limited but nitrogen replete growth conditions. The lipid ratio of all the strains decreased with the introduction of silicon availability. For instance, *T.weissflogii* 1336 had a lipid content of about 40% at the beginning of Stage II and following silicon dosages this value went down to about 15% and did not increase to previous levels even after silicon depletion. The lipid content of *T.pseudonana* 122.79 followed a similar trend: lipid content decreased from 30% down to about 15% following silicon availability and stayed at that level. *T. pseudonana* 122.79 was an exceptional lipid producer. This exceptionality comes from the strains's ability to reach a lipid content exceeding 45% both at the beginning and end of stage II and also having a minimum lipid content of 35% even under silicon availability.

The highest chitin contents achieved were about 4%, 7%, and 15% with *T.pseudonana* 122.79, *T.weissflogii* 1336, and *T.pseudonana* 2135. Biomass chitin content increased drastically following the silicon depletion in the aqueous phase, particularly for *T.pseudonana* 122.79, and *T.weissflogii* 1336. *T.pseudonana* 2135 had the highest lipid and chitin contents at the end of the cultivation.

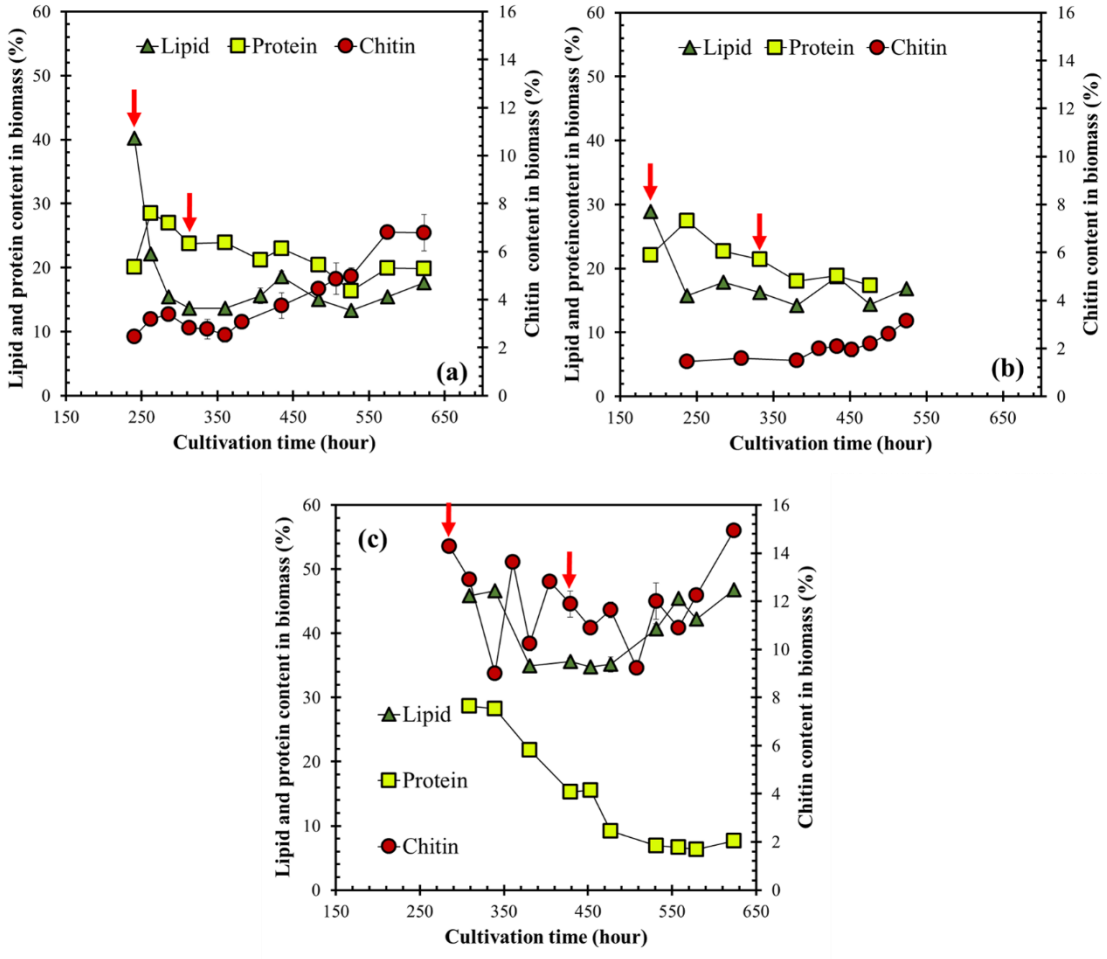

Figure 11. Lipid, protein, and chitin content in biomass (%) during Stage II cultivation process for all strains, (a) *T.weissflogii* 1336, (b) *T.pseudonana* 122.79, and (c) *T.pseudonana* 2135. The arrows mean the first silicon dosage and last silicon dosage.

4.5. Fatty acids

Figure 12 presents the fatty acid distributions of the strains in the stationary phase of the second growth stage following transesterification. The long-chain polyunsaturated fatty acids (LCPUFAs) content, particularly eicosapentaenoic (EPA) (20:5,n-3) and docosahexaenoic acid (DHA) (22:6,n-3) acid, is the primary biochemical parameter that controls the applicability of diatom cells as live feed in the aquaculture industry. All the strains cultivated produced these critical fatty acids to varying degrees. *T. weissflogii* strain was quite rich in LCPUFAs content and had a cumulative ratio of more than 25%.

T. pseudonana 2135 had the lowest ratio but had palmitic (16:0) and palmitoleic acids (16:1) accounted for more than 75% of the fatty acids. Fatty acids composition results are listed in Appendix A2. Lipids containing C16 fatty acids can be more readily used for biodiesel production (Jeon et al. 2022). Thus, *T. pseudonana* 2135 biomass shows good potential for use as diesel feedstock material when its C16-rich fatty acid profile and also high dry biomass lipid content are taken into the account.

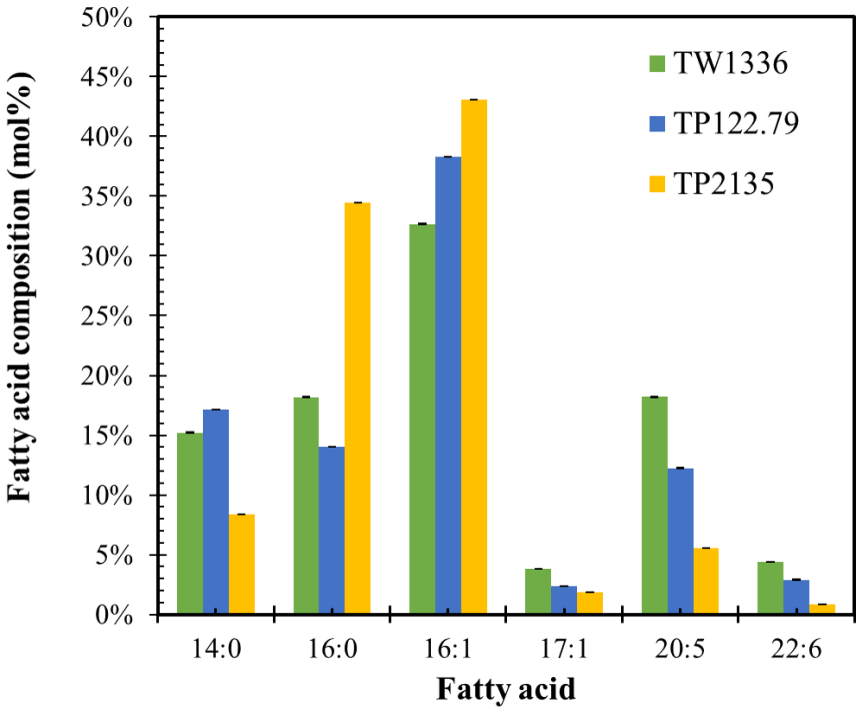

Figure 12. Fatty acid composition of *Thalassiosira* strains at stationary growth phase of Stage II.

CHAPTER 5

CONCLUSION

Diatom species belonging to *Cyclotella* and *Thalassiosira* genera are unique with their ability to biosynthesize chitin nanofibers and extrude them from their cell walls. In this study, three diatom strains that belong to *Thalassiosira* genera were cultivated in a bubble column photobioreactor under silicon deplete and replete conditions to determine and compare the chitin productivity metrics of industrial interest. This is the first study that cultivates *Thalassiosira* strains under standard process conditions in a photobioreactor and analyzes the chitin productivity metrics of commercial interest. Co-production of other commercially valuable metabolites was also investigated with the aim to diversify the product portfolio and improve economics. These co-products included lipids, proteins, and fatty acids. These analyses also served to assess the commercial potential of these strains as live feed in the aquaculture industry.

Chitin productivity changed significantly between the strains tested, showing the importance of strain selection for industrial-scale production of this metabolite. *T. pseudonana* 2135 strain had the highest peak production rate, final chitin concentration, and average fiber diameter. Silicon depletion increased the chitin biosynthesis in *T. weissflogii* 1336 and *T. pseudonana* 122.79. Biomass chitin contents ranged from about 4% to 15%.

At the beginning of the second stage, the protein content in the biomass reached approximately 30% in all strains and decreased towards the end of the cultivation period. For example, the biomass protein ratio of *T. weissflogii* 1336 increased from about 20% to 30% with the addition of the first silicon dose. It then decreased to 20% during the following cultivation period. *T. pseudonana* 122.79 strain also showed a similar profile: with the addition of silicon, the protein content first increased and then decreased

At the beginning of Stage II, the lipid content in *T. weissflogii* 1336 and *T. pseudonana* 122.79 strains was 40% and 30%, respectively. After the first dose of silicon, the amount of lipid in these two strains decreased drastically to about 15% and stayed at that level until the end of the experiments. *T. pseudonana* 122.79 varied from the others by having a higher lipid content throughout the 2nd growth stage and having minimum and maximum lipids content of 35% and 50%, respectively. Fatty acid profiles pointed

out to potential uses for different applications. C16 fatty acids accounted for more than 75% of the fatty acids biosynthesized by *T. pseudonana* 2135, showing suitability for use in biodiesel production. EPA and DHA accounted for more than 25% of the fatty acids in the *T. weissflogii* strain. These fatty acids are the biomass constituents that govern the applicability as live feed in the aquaculture industry. Thus, this strain has the potential to sustain a biorefinery that can simultaneously generate chitin nanofibers and aquaculture feed.

REFERENCES

Aranaz, Inmaculada, Marian Mengibar, Ruth Harris, Ines Panos, Beatriz Miralles, Niuris Acosta, Gemma Galed, and Angeles Heras. 2009. "Functional Characterization of Chitin and Chitosan." *Current Chemical Biology* 3 (2): 203–30. https://doi.org/10.2174/187231309788166415.

Barahoei, Malihe, Mohammad Sadegh, and Saeed Afsharzadeh. 2020. "CO 2 Capturing by Chlorella Vulgaris in a Bubble Column Photo-Bioreactor ; Effect of Bubble Size on CO2 Removal and Growth Rate." *Journal of CO2 Utilization* 37 (November 2019): 9–19. https://doi.org/10.1016/j.jcou.2019.11.023.

Barclay, W. R., K. M. Meager, and J. R. Abril. 1994. "Heterotrophic Production of Long Chain Omega-3 Fatty Acids Utilizing Algae and Algae-like Microorganisms." *Journal of Applied Phycology* 6 (2): 123–29. https://doi.org/10.1007/BF02186066.

Belarbi, El Hassan, Emilio Molina, and Yusuf Chisti. 2000. "A Process for High Yield and Scaleable Recovery of High Purity Eicosapentaenoic Acid Esters from Microalgae and Fish Oil." *Enzyme and Microbial Technology* 26 (7): 516–29. https://doi.org/10.1016/S0141-0229(99)00191-X.

Bozarth, Andrew, Uwe G. Maier, and Stefan Zauner. 2009. "Diatoms in Biotechnology: Modern Tools and Applications." *Applied Microbiology and Biotechnology* 82 (2): 195–201. https://doi.org/10.1007/s00253-008-1804-8.

Bradford, Marion M. 1976. "A Rapid And Sensitive Method for the Quantitation of Microgram Quantities of Protein Utilizing the Principle of Protein-Dye Binding." *Crop Journal* 5 (5): 248–53. https://doi.org/10.1016/j.cj.2017.04.003.

Cerón Garcí, M. C., J. M. Fernández Sevilla, F. G. Acién Fernández, E. Molina Grima, and F. García Camacho. 2000. "Mixotrophic Growth of Phaeodactylum Tricornutum on Glycerol: Growth Rate and Fatty Acid Profile." *Journal of Applied*

Phycology 12 (3–5): 239–48. https://doi.org/10.1023/a:1008123000002.

Chiriboga, Omar G, and Gregory L Rorrer. 2017. "Control of Chitin Nanofiber Production by the Lipid-Producing Diatom Cyclotella Sp . Through Fed-Batch Addition of Dissolved Silicon and Nitrate in a Bubble-Column Photobioreactor." https://doi.org/10.1002/btpr.2445.

Chiriboga, Omar, and Gregory L Rorrer. 2018. "Effects of Nitrogen Delivery on Chitin Nanofiber Production during Batch Cultivation of the Diatom Cyclotella Sp . in a Bubble Column Photobioreactor," 1575–81.

Chisti, Yusuf. 2007. "Biodiesel from Microalgae." *Biotechnology Advances* 25 (3): 294–306. https://doi.org/10.1016/j.biotechadv.2007.02.001.

Chu, Wan Loy, Siew Moi Phang, and Swee Hock Goh. 1994. "Studies on the Production of Useful Chemicals, Especially Fatty Acids in the Marine Diatom Nitzschia Conspicua Grunow." *Hydrobiologia* 285 (1–3): 33–40. https://doi.org/10.1007/BF00005651.

Cohen, Zvi, and Colin Ratledge. 2005. *Single Cell Oils: Microbial and Algal Oils*. AOCS Publishing.

Collos, Y, F Mornet, A Sciandra, N Waser, A Larson, and P.J. Harrison. 1999. "An Optical Method for the Rapid Measurement of Nitrate in Marine Phytoplankton Cultures." *Journal of Applied Phycology* 11: 179–84. https://doi.org/https://doi.org/10.1023/A:1008046023487.

D'Ippolito, Giuliana, Angela Sardo, Debora Paris, Filomena Monica Vella, Maria Grazia Adelfi, Pierpaolo Botte, Carmela Gallo, and Angelo Fontana. 2015. "Potential of Lipid Metabolism in Marine Diatoms for Biofuel Production." *Biotechnology for Biofuels* 8 (1): 1–10. https://doi.org/10.1186/s13068-015-0212-4.

Dweltz, N.E., J.R. Colvin, and A.G. McInnes. 1968. “Studies on Chitan (B-(1-4)-Linked 2-Acetamido-2-Deoxy-D-Glucan) Fibers of the Diatom *Thalassiosira Fluviatilis*, Hustedt. III The Structure of Chitan from x-Ray Diffraction and Electron Microscope Observations.” *Canadian Journal of Chemistry* 46: 1513–21. https://doi.org/https://doi.org/10.1139/v68-248.

Enzing, Christien, Matthias Ploeg, Maria Barbosa, and Lolke Sijtsma. 2014. *Microalgae-Based Products for the Food and Feed Sector: An Outlook for Europe*. *JRC Scientific and Policy Reports*. https://doi.org/10.2791/3339.

Ewy, Matthew W., Ankitaben Patel, Marwa G. Abdelmagid, Osman Mohamed Elfadil, Sara L. Bonnes, Bradley R. Salonen, Ryan T. Hurt, and Manpreet S. Mundi. 2022. “Plant-Based Diet: Is It as Good as an Animal-Based Diet When It Comes to Protein?” *Current Nutrition Reports* 11 (2): 337–46. https://doi.org/10.1007/s13668-022-00401-8.

Fanning, Kent A., and Michael E.Q. Pilson. 1973. “On the Spectrophotometric Determination of Dissolved Silica in Natural Waters.” *Analytical Chemistry* 45 (1): 136–40. https://doi.org/10.1021/ac60323a021.

Geada, Pedro, Catarina Moreira, Maria Silva, Rafaela Nunes, Leandro Madureira, Cristina M.R. Rocha, Ricardo N. Pereira, António A. Vicente, and José A. Teixeira. 2021. “Algal Proteins: Production Strategies and Nutritional and Functional Properties.” *Bioresource Technology* 332 (February). https://doi.org/10.1016/j.biortech.2021.125125.

Gooday, Graham W., Julia Woodman, Elizabeth A. Casson, and Catherine A. Browne. 1985. “Effect of Nikkomycin on Chitin Spine Formation in the Diatom Thalassiosira Fluviatilis, and Observations on Its Peptide Uptake.” *FEMS Microbiology Letters* 28 (3): 335–40. https://doi.org/10.1111/j.1574-6968.1985.tb00816.x.

Gordon, Jeffrey M, and Juergen E W Polle. 2007. “Ultrahigh Bioproductivity from Algae.” *Applied Microbiology and Biotechnology* 76 (5): 969–75.

Gouveia, L., A. P. Batista, I. Sousa, A. Raymundo, and N. M. Bandarra. 2009. *Microalgae in Novel Food Products. Algae: Nutrition, Pollution Control and Energy Sources.*

Graham, James M., Linda E. Graham, Shahrizim B. Zulkifly, Brian F. Pfleger, Spencer W. Hoover, and Jun Yoshitani. 2012. "Freshwater Diatoms as a Source of Lipids for Biofuels." *Journal of Industrial Microbiology and Biotechnology* 39 (3): 419–28. https://doi.org/10.1007/s10295-011-1041-5.

Gupta, Prabuddha L., Seung Mok Lee, and Hee Jeong Choi. 2015. "A Mini Review: Photobioreactors for Large Scale Algal Cultivation." *World Journal of Microbiology and Biotechnology* 31 (9): 1409–17. https://doi.org/10.1007/s11274-015-1892-4.

Jeon, Kyung-Won, Ho-Ryong Park, Yeol-Lim Lee, Jee-Eun Kim, Won-Jun Jang, Jae-Oh Shim, and Hyun-Seog Roh. 2022. "Deoxygenation of Non-Edible Fatty Acid for Green Diesel Production: Effect of Metal Loading Amount over Ni/MgO–Al2O3 on the Catalytic Performance and Reaction Pathway." *Fuel* 311: 122488.

Kanamoto, Akihiko, Yuichi Kato, Erina Yoshida, Tomohisa Hasunuma, and Akihiko Kondo. 2021. "Development of a Method for Fucoxanthin Production Using the Haptophyte Marine Microalga Pavlova Sp. OPMS 30543." *Marine Biotechnology* 23 (2): 331–41. https://doi.org/10.1007/s10126-021-10028-5.

Khan, Muhammad Imran, Jin Hyuk Shin, and Jong Deog Kim. 2018. "The Promising Future of Microalgae: Current Status, Challenges, and Optimization of a Sustainable and Renewable Industry for Biofuels, Feed, and Other Products." *Microbial Cell Factories* 17 (1): 1–21. https://doi.org/10.1186/s12934-018-0879-x.

Koyande, Apurav Krishna, Kit Wayne Chew, Krishnamoorthy Rambabu, Yang Tao, Dinh Toi Chu, and Pau Loke Show. 2019. "Microalgae: A Potential Alternative to Health Supplementation for Humans." *Food Science and Human Wellness* 8 (1): 16–24. https://doi.org/10.1016/j.fshw.2019.03.001.

Kuczynska, Paulina, Malgorzata Jemiola-Rzeminska, and Kazimierz Strzalka. 2015. "Photosynthetic Pigments in Diatoms." *Marine Drugs* 13 (9): 5847–81.

Lavens, Patrick, and Patrick Sorgeloos. 1996. *Manual on the Production and Use of Live Food for Aquaculture*. *Fao Fisheries Technical Paper*. Vol. 361.

Lebeau, T., and J. M. Robert. 2003a. "Diatom Cultivation and Biotechnologically Relevant Products. Part II: Current and Putative Products." *Applied Microbiology and Biotechnology*. https://doi.org/10.1007/s00253-002-1177-3.

Lebeau, T., and J.M. Robert. 2003b. "Diatom Cultivation and Biotechnologically Relevant Products. Part I: Cultivation at Various Scales." *Applied Microbiology and Biotechnology* 60 (60): 612–23. https://doi.org/10.1007/s00253-002-1177-3.

Lebeau, Thierry, and Jean Michel Robert. 2003. "Diatom Cultivation and Biotechnologically Relevant Products. Part I: Cultivation at Various Scales." *Applied Microbiology and Biotechnology* 60 (6): 612–23. https://doi.org/10.1007/s00253-002-1176-4.

LeDuff, Paul, and Gregory L. Rorrer. 2019a. "Formation of Extracellular β-Chitin Nanofibers during Batch Cultivation of Marine Diatom Cyclotella Sp. at Silicon Limitation." *Journal of Applied Phycology* 31 (6): 3479–90. https://doi.org/10.1007/s10811-019-01879-6.

LeDuff, Paul, and Gregory L. Rorrer. 2019b. "Formation of Extracellular β-Chitin Nanofibers during Batch Cultivation of Marine Diatom *Cyclotella* Sp. at Silicon Limitation." *Journal of Applied Phycology* 31 (6): 3479–90. https://doi.org/10.1007/s10811-019-01879-6.

Lucas, John S, Paul C Southgate, and Craig S Tucker. 2019. *Aquaculture: Farming Aquatic Animals and Plants*. John Wiley & Sons.

M. S. Rao, J. Muñoz & W. F. Stevens. 2000. “Critical Factors in Chitin Production by Fermentation of Shrimp Biowaste.” *Applied Microbiology and Biotechnology Volume* 54: 808–13.

Metcalfe, L D, A A Schmitz, and J R Pelka. 1966. “Rapid Preparation of Fatty Acid Esters from Lipids for Gas Chromatographic Analysis.” *Analytical Chemistry* 38 (3): 514–15.

Milledge, John J. 2011. “Commercial Application of Microalgae Other than as Biofuels: A Brief Review.” *Reviews in Environmental Science and Biotechnology* 10 (1): 31–41. https://doi.org/10.1007/s11157-010-9214-7.

Morin, Linda G., Richard A. Smucker, and Werner Herth. 1986. “Effects of Two Chitin Synthesis Inhibitors on Thalassiosira Fluviatilis and Cyclotella Cryptica.” *FEMS Microbiology Letters* 37 (3): 263–68. https://doi.org/10.1111/j.1574-6968.1986.tb01806.x.

Ozkan, Altan, and Gregory L. Rorrer. 2017a. “Effects of CO2 Delivery on Fatty Acid and Chitin Nanofiber Production during Photobioreactor Cultivation of the Marine Diatom Cyclotella Sp.” *Algal Research*. https://doi.org/10.1016/j.algal.2017.07.003.

Ozkan, Altan, and Gregory L. Rorrer. 2017b. “Lipid and Chitin Nanofiber Production during Cultivation of the Marine Diatom Cyclotella Sp. to High Cell Density with Multistage Addition of Silicon and Nitrate.” *Journal of Applied Phycology*. https://doi.org/10.1007/s10811-017-1113-7.

Ozkan, Altan, and Gregory L Rorrer. 2017c. “Effects of Light Intensity on the Selectivity of Lipid and Chitin Nano Fi Ber Production during Photobioreactor Cultivation of the Marine Diatom.” *Algal Research* 25 (March): 216–27. https://doi.org/10.1016/j.algal.2017.04.032.

Ruiz-Lopez, Noemi, Sarah Usher, Olga V. Sayanova, Johnathan A. Napier, and Richard P. Haslam. 2015. “Modifying the Lipid Content and Composition of Plant Seeds: Engineering the Production of LC-PUFA.” *Applied Microbiology and Biotechnology* 99 (1): 143–54. https://doi.org/10.1007/s00253-014-6217-2.

Shi, Jing, Lisong Yang, and Colin D Bain. 2019. “Drying of Ethanol/Water Droplets Containing Silica Nanoparticles.” https://doi.org/10.1021/acsami.8b21731.

Soni, Ruma Arora, K. Sudhakar, and R. S. Rana. 2017. “Spirulina – From Growth to Nutritional Product: A Review.” *Trends in Food Science and Technology* 69 (September): 157–71. https://doi.org/10.1016/j.tifs.2017.09.010.

Tocher, Douglas R., Monica B. Betancor, Matthew Sprague, Rolf E. Olsen, and Johnathan A. Napier. 2019. “Omega-3 Long-Chain Polyunsaturated Fatty Acids, EPA and DHA: Bridging the Gap between Supply and Demand.” *Nutrients* 11 (1): 1–20. https://doi.org/10.3390/nu11010089.

Tréguer, Paul, David M. Nelson, Aleido J. Van Bennekom, David J. Demaster, Aude Leynaert, and Bernard Quéguiner. 1995. “The Silica Balance in the World Ocean: A Reestimate.” *Science* 268 (5209): 375–79. https://doi.org/10.1126/science.268.5209.375.

Ugwu, C. U., H. Aoyagi, and H. Uchiyama. 2008. “Photobioreactors for Mass Cultivation of Algae.” *Bioresource Technology* 99 (10): 4021–28. https://doi.org/10.1016/j.biortech.2007.01.046.

Wen, Zhi You, and Feng Chen. 2000. “Production Potential of Eicosapentaenoic Acid by the Diatom Nitzschia Laevis.” *Biotechnology Letters* 22 (9): 727–33. https://doi.org/10.1023/A:1005666219163.

Xiang, Xuwen, Altan Ozkan, Omar Chiriboga, Nattaporn Chotyakul, and Christine Kelly. 2017. “Techno-Economic Analysis of Glucosamine and Lipid Production from Marine Diatom Cyclotella Sp.” *Bioresource Technology*. https://doi.org/10.1016/j.biortech.2017.05.079.

Ye, Chensong, Dongyan Mu, Naomi Horowitz, Zhonglin Xue, Jie Chen, Mingxiong Xue, Yu Zhou, Megan Klutts, and Wenguang Zhou. 2018. “Life Cycle Assessment of Industrial Scale Production of Spirulina Tablets.” *Algal Research* 34 (May): 154–63. https://doi.org/10.1016/j.algal.2018.07.013.

Zhou, Yingdong, Li Liu, Mingyu Li, and Changwei Hu. 2022. “Algal Biomass Valorisation to High-Value Chemicals and Bioproducts: Recent Advances, Opportunities and Challenges.” *Bioresource Technology* 344 (PB): 126371. https://doi.org/10.1016/j.biortech.2021.126371.

Zulu, Nodumo Nokulunga, Krzysztof Zienkiewicz, Katharina Vollheyde, and Ivo Feussner. 2018. “Current Trends to Comprehend Lipid Metabolism in Diatoms.” *Progress in Lipid Research* 70 (March): 1–16. https://doi.org/10.1016/j.plipres.2018.03.001.

APPENDIX A

A1. Optical Densities at 750 nm, 680 nm, and 530 nm for (a) *T. weissflogii* 1336, (b) *T. pseudonana* 122.79, and (c) *T. pseudonana* 2135 strains

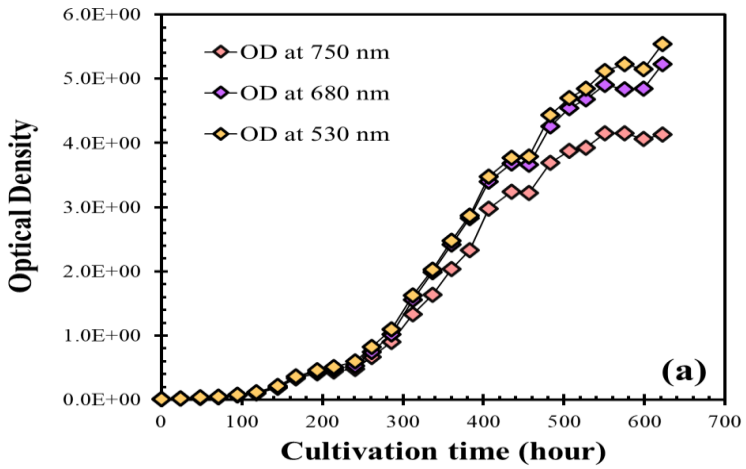

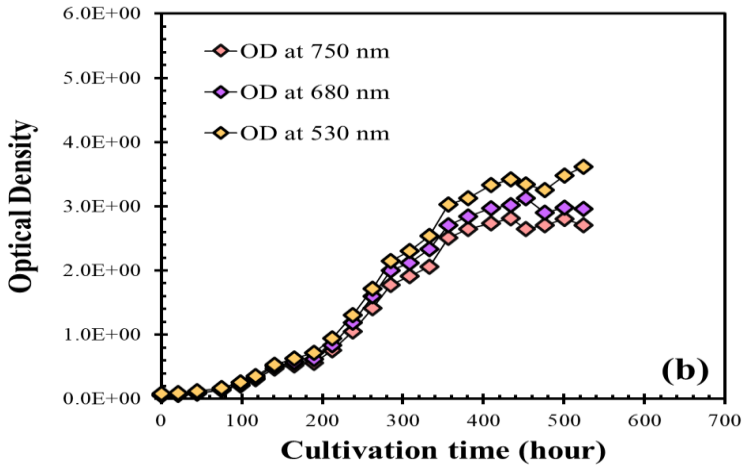

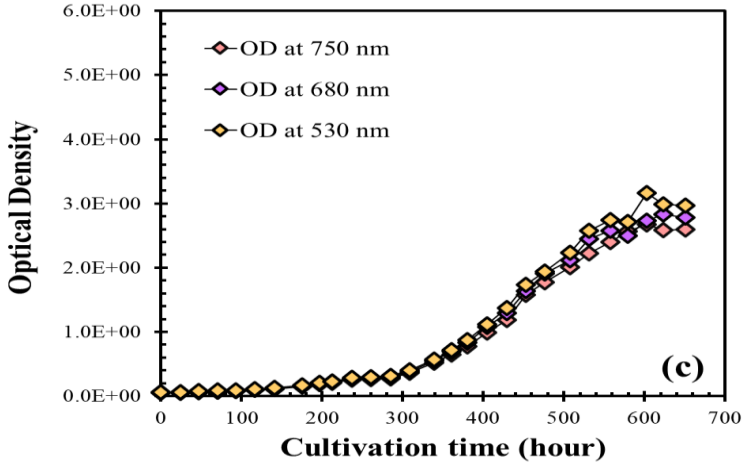

A2. Fatty acids compositions

Analyze	TW1336			TP122.79			TP2135		
	%	Avg	Std Err	%	Avg	Std Err	%	Avg	Std Err
n1: C14:0 Myristic acid	15	15	0.05	17	17	0.02	8.4	8.4	0.01
n2: C14:0 Myristic acid	15			17			8.3		
n1: C15:0 Pentadecanoic acid	1.2	1.2	0	1	0.9	0.01	1	1	0
n2: C15:0 Pentadecanoic acid	1.2			1			1		
n1: C16:0 Palmitic acid	18	18	0.02	14	14	0.02	34	34	0.01
n2: C16:0 Palmitic acid	18			14			34		
n1: C16:1 Palmitoleic acid	33	33	0.035	38	38	0.02	43	43	0.01
n2: C16:1 Palmitoleic acid	33			38			43		
n1: C17:0 Margaric acid	0	0	0	0	0.1	0	0.1	0.1	0
n2: C17:0 Margaric acid	0			0			0.1		
n1: C17:1 Heptadecenoic Acid	3.8	3.8	0.005	2	2.4	0	1.8	1.8	0
n2: C17:1 Heptadecenoic Acid	3.8			2			1.8		
n1: C18:0 Stearic Acid	1.5	1.5	0.005	2	1.6	0.01	0.6	0.6	0
n2: C18:0 Stearic Acid	1.5			2			0.6		
n1: C18:1n+9c Oleic acid	1.8	1.8	0	2	2.1	0.01	0.5	0.5	0
n2: C18:1n+9c Oleic acid	1.8			2			0.5		
n1: C18:2n+6c yLinoleic acid	1	0.9	0.045	2	1.9	0	1.5	1.5	0
n2: C18:2n+6c yLinoleic acid	0.9			2			1.5		
n1: C18:3n-3 Linolenic acid	0	0	0	0	0.1	0	2.1	2.1	0
n2: C18:3n-3 Linolenic acid	0			0			2.1		

(cont. on next page)

A2. (cont.)

n1: C18:3n-6 yLinolenic acid	0.5	0.5	0.005	1	0.8	0	0.1	0.1	0.01
n2: C18:3n-6 yLinolenic acid	0.5			1			0.1		
n1: C20:0 Arachidic acid	0.2	0.2	0	0	0.1	0	0	0	0
n2: C20:0 Arachidic acid	0.2			0			0		
n1: C20:1 Eicosenoic acid	0.3	0.3	0.02	0	0.1	0.01	0	0	0
n2: C20:1 Eicosenoic acid	0.3			0			0		
n1: C20:3n6 cis-8.11.14-Eicosatrienoic acid	0	0	0	0	0.5	0.01	0	0	0
n2: C20:3n6 cis-8.11.14-Eicosatrienoic acid	0			0			0		
n1: C20:4n6 Arachiodonic acid	0	0	0	3	3.2	0.02	0	0	0
n2: C20:4n6 Arachiodonic acid	0			3			0		
n1: C20:5n3 Eicosapentaenoic acid	18	18	0.03	12	12	0.03	5.6	5.6	0.01
n2: C20:5n3 Eicosapentaenoic acid	18			12			5.6		
n1: C21:0 Heleicosanoic acid	0.4	0.4	0.005	0	0.3	0	0.1	0.1	0
n2: C21:0 Heleicosanoic acid	0.4			0			0.1		
n1: C22:0 Behenic acid	0	0	0	0	0.4	0	0	0	0
n2: C22:0 Behenic acid	0			0			0		
n1: C22:6n3 Docosahexaenoic acid	4.4	4.4	0.01	3	2.9	0.01	0.8	0.8	0
n2: C22:6n3 Docosahexaenoic acid	4.4			3			0.8		
n1: C24:0 Lignoceric Acid	0.7	0.7	0.005	1	0.9	0.01	0	0	0
n2: C24:0 Lignoceric Acid	0.7			1			0		